© 2014. Published by The Company of Biologists Ltd | Development (2014) 141, 650-660 doi:10.1242/dev.099655

RESEARCH ARTICLE

Dendrite architecture organized by transcriptional control of the F-actin nucleator Spire

Tiago Ferreira[1,*], Yimiao Ou[1,2,*], Sally Li[1], Edward Giniger[3] and Donald J. van Meyel[1,2,4,5,‡]

ABSTRACT

The architectures of dendritic trees are crucial for the wiring and function of neuronal circuits because they determine coverage of receptive territories, as well as the nature and strength of sensory or synaptic inputs. Here, we describe a cell-intrinsic pathway sculpting dendritic arborization (da) neurons in *Drosophila* that requires Longitudinals Lacking (Lola), a BTB/POZ transcription factor, and its control of the F-actin cytoskeleton through Spire (Spir), an actin nucleation protein. Loss of Lola from da neurons reduced the overall length of dendritic arbors, increased the expression of Spir, and produced inappropriate F-actin-rich dendrites at positions too near the cell soma. Selective removal of Lola from only class IV da neurons decreased the evasive responses of larvae to nociception. The increased Spir expression contributed to the abnormal F-actin-rich dendrites and the decreased nocifensive responses because both were suppressed by reduced dose of Spir. Thus, an important role of Lola is to limit expression of Spir to appropriate levels within da neurons. We found Spir to be expressed in dendritic arbors and to be important for their development. Removal of Spir from class IV da neurons reduced F-actin levels and total branch number, shifted the position of greatest branch density away from the cell soma, and compromised nocifensive behavior. We conclude that the Lola-Spir pathway is crucial for the spatial arrangement of branches within dendritic trees and for neural circuit function because it provides balanced control of the F-actin cytoskeleton.

KEY WORDS: Neuron, *Drosophila*, Dendrite, Arborization, F-actin, Nociception, Sholl

INTRODUCTION

Neurons receive sensory and synaptic input through their dendrites, and proper architecture of dendritic trees is instrumental for neuronal function (Jan and Jan, 2010; Hall and Treinin, 2011). Dendritic trees are crucial determinants of the type-specific properties of neurons. They define the coverage of receptive territories, they contribute to the specificity of connections with presynaptic axons and they influence the number, strength and integration of inputs. Therefore, an important issue in neurobiology is to understand what factors control the location and degree of branching within dendritic trees.

[1]McGill Centre for Research in Neuroscience, McGill University Health Centre, 1650 Cedar Avenue, Montreal, QC H3G 1A4, Canada. [2]Integrated Program in Neuroscience, McGill University, Montreal, QC H3A 2B4, Canada. [3]Basic Neuroscience Program, National Institute of Neurological Disorders and Stroke, National Institutes of Health, Bethesda, MD 20892, USA. [4]Department of Neurology and Neurosurgery, McGill University, 3801 University Street, Room 144, Montreal, QC H3A 2B4, Canada. [5]McGill University Health Centre Research Institute, 1650 Cedar Avenue, Montreal, QC H3G 1A4, Canada.
*These authors contributed equally to this work

‡Author for correspondence (don.vanmeyel@mcgill.ca)

Received 30 May 2013; Accepted 12 November 2013

Intrinsic control by transcription factors has emerged as an important mechanism that regulates the branching patterns of dendrites (Parrish et al., 2006; Ou et al., 2008; Jan and Jan, 2010; Smith et al., 2010; de la Torre-Ubieta and Bonni, 2011). However, it remains largely unknown how they influence the dynamic remodeling of the dendritic cytoskeleton that accompanies branching and outgrowth, as scant progress has been made in linking these transcription factors to key effectors that control rearrangements of actin filaments (F-actin) and microtubules (MTs). F-actin and MTs are major structural components of dendrites that support the transport by motor proteins of organelles and macromolecular complexes that are used to build and maintain arbors. In addition, F-actin is the major constituent of dendritic filopodia, finger-like projections that initiate branch outgrowth. Cellular F-actin is known to be assembled from actin monomers by a range of proteins that nucleate filaments, regulate their elongation and turnover, and crosslink them into networks or bundles (Pollard and Cooper, 2009). However, key F-actin regulators in dendrites that contribute to where and how branches are spatially organized remain unclear, particularly *in vivo*, where arbors grow within their native cellular context.

Here, we have investigated this in the dendritic arborization (da) neurons of the *Drosophila* peripheral nervous system (PNS), which extend dendrites in the larval body wall between muscles and epithelial cells (Grueber et al., 2002). Branching and elongation of da neuron dendrites begins in embryogenesis and continues in larval stages, where F-actin is enriched at the tips of nascent or growing branches but is also found along shafts and at branch points (Medina et al., 2006; Nagel et al., 2012). Individual da neurons are identifiable and their patterns of dendrite outgrowth are largely invariant from embryo to embryo (Gao et al., 1999), allowing one to readily detect and measure changes that are induced experimentally. One can correlate these changes with the capacity of some of these sensory neurons to respond specifically to known stimuli (Tracey et al., 2003; Tsubouchi et al., 2012; Yan et al., 2013), thereby linking cellular and molecular mechanisms of dendrite arborization with neuronal physiology and animal behavior.

In a screen for genes that influence dendrite patterning (Ou et al., 2008), we identified *longitudinals-lacking* (*lola*), which encodes a BTB-Zn-finger transcription factor (Lola). Lola has been shown to regulate axon guidance in the CNS and PNS (Giniger et al., 1994; Kania et al., 1995; Crowner et al., 2002), cell fate in the developing eye (Zheng and Carthew, 2008), and neuronal identity in the olfactory system (Spletter et al., 2007). Here, we find that Lola is required for sculpting dendritic arbors in da neurons, and that it does so by controlling the expression of Spire (Spir), a conserved member of the WASP homology 2 (WH2)-domain family of actin nucleation factors. Actin nucleators overcome the kinetic barrier to spontaneous actin polymerization and so they are key rate-limiting factors for the spatial and temporal regulation of actin dynamics (Pollard and Cooper, 2009). Spir and its related proteins in mammals have

Development (2014) doi:10.1242/dev.099655

previously been shown to nucleate, sever and cap actin filaments at their barbed ends, and to synergize with Profilin and Formin proteins to enhance processive filament assembly (Quinlan et al., 2005; Bosch et al., 2007). Spir had been identified previously as a Lola effector involved in motor axon guidance (Gates et al., 2011), but a role for either Lola or Spir in dendrite morphogenesis has not been described. We find that a Lola-Spir pathway shapes dendrite architecture by controlling the formation of branches, the abundance of F-actin in those branches and their spatial arrangement. We also discover that Lola and Spir are required in da neurons for accurate escape responses to nociception (Tracey et al., 2003), correlating their role in sculpting dendritic trees with neuronal function and behavioral performance.

RESULTS

Lola is expressed in sensory neurons and required for evasive responses to nociception

da neurons belong to one of four classes (I-IV) of increasing dendritic complexity and size, with class I da neurons having simple polarized arbors and class IV da neurons having very large and highly complex radial arbors (Grueber et al., 2002). Using immunohistochemistry in third instar (L3) larvae, we found that Lola was expressed in the nuclei of all da neurons (Fig. 1A-B″). This staining was specific because it was not detected in da neurons homozygous for *lola*^{ore76}, a null allele (Fig. 1C-C″). Furthermore, Lola expression was eliminated using RNA interference (RNAi) to selectively knock down Lola expression in class IV da neurons with *ppk1.9-GAL4* and a single RNAi-inducing transgene for Lola (Fig. 1D-D″) (Dietzl et al., 2007).

In L3 larvae, class IV da neurons mediate an escape response to noxious thermal (45°C) and mechanical stimulation that is characterized by rotation around the anteroposterior axis (Tracey et al., 2003). The latency to initiate this nocifensive escape locomotion (NEL) is a measure of larval responsiveness. To determine whether Lola was required specifically in class IV da neurons for this response, we compared controls with *lola* RNAi knockdown. All control larvae responded within 20 seconds, and the mean latency was 3.1 seconds (Fig. 1E). By contrast, 21.1% of *lola* RNAi animals did not respond within 20 seconds, and the mean latency was 10.4 seconds.

Lola is required for the appropriate number and arrangement of dendrite branches

These reduced nocifensive responses in *lola* RNAi animals could arise from neuroanatomical defects and/or physiological impairment of class IV da neurons. To investigate the possibility of defects in axon guidance, we used reporters to trace axon projections of class IV da neurons to their terminations within the CNS of L3 larvae, but found that the patterns in controls and *lola* RNAi were indistinguishable (Fig. 1F,G; supplementary material Fig. S1). In addition, we used optogenetic activation of nocifensive behavior (Hwang et al., 2007; Honjo et al., 2012). Channelrhodopsin 2 (ChR-2::YFP) was expressed specifically within class IV da neurons, and we found that controls and *lola* RNAi animals responded identically with robust nocifensive escape responses to light activation (Fig. 1H), indicating that the integrity of sensory axon projections and their synaptic contacts within the CNS were largely intact.

As optogenetic activation with ChR-2 bypasses sensory transduction by dendrites, we addressed the interesting possibility that the nocifensive defect in *lola* RNAi animals could be due instead to an undiscovered role for Lola in dendrite morphogenesis. We began by examining the mCD8::GFP-labeled

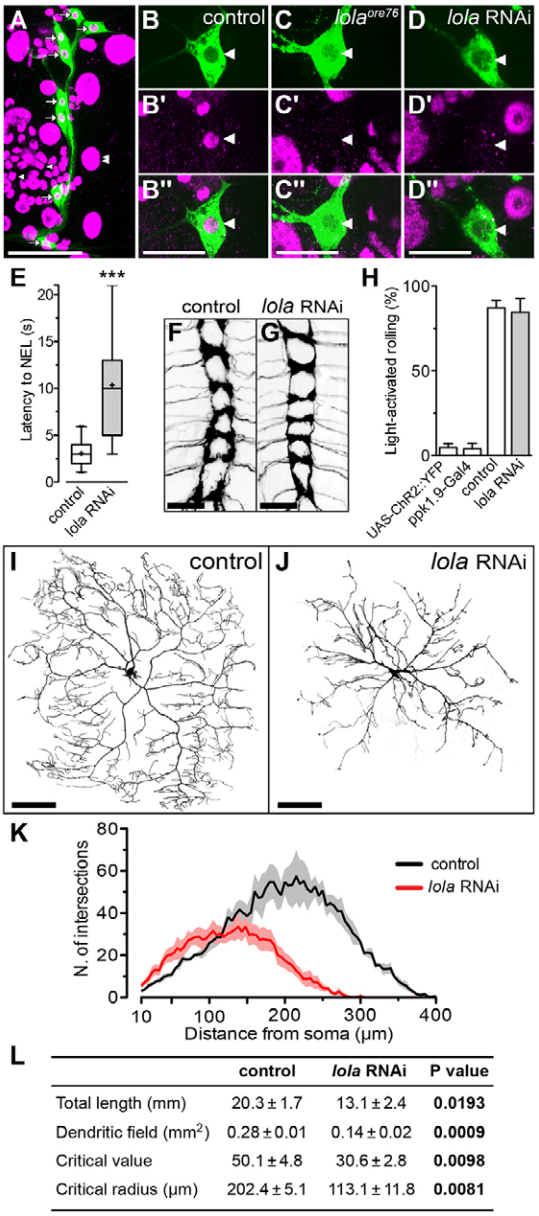

L

	control	*lola* RNAi	P value
Total length (mm)	20.3±1.7	13.1±2.4	**0.0193**
Dendritic field (mm^2)	0.28±0.01	0.14±0.02	**0.0009**
Critical value	50.1±4.8	30.6±2.8	**0.0098**
Critical radius (µm)	202.4±5.1	113.1±11.8	**0.0081**

Fig. 1. Lola is required in class IV da neurons for appropriate dendrite arborization and nocifensive behavior. (A) Dorsal da neurons of L3 larvae (green) labeled by GAL4$^{109(2)80}$-driven mCD8::GFP. Lola immunoreactivity (magenta) was observed in all da neurons (arrows), as well as in muscles (arrowheads) and epithelia (double arrowhead). (B-B″) Lola immunoreactivity in the nucleus of a control MARCM clone of a class IV da neuron (ddaC, arrowheads) labeled with mCD8::GFP. (C-C″) Lola is absent from a *lola*^{ore76} homozygous ddaC clone (arrowheads). (D-D″) Lola is absent following knockdown from a GFP-labeled ddaC (arrowheads) using *ppk1.9-GAL4*-driven RNAi. (E-L) Effects of RNAi knockdown. (E) Boxplot of latencies to initiate nocifensive escape locomotion (NEL) from a thermal probe at 45°C (*t*-test, $P<0.0001$; controls, $n=20$; *lola* RNAi, $n=19$). (F,G) Axon terminals of ppk-CD4::tdTomato-labeled class IV da neurons (L3 larvae) appear unaffected by *lola* RNAi. (H) Evoked nocifensive behavior with ChR2. Blue light-activated rolling of control larvae (87.14±4.24%, $n=107$) was indistinguishable from *lola* RNAi animals (84.56±8.00%, $n=78$). Also shown are baseline levels of rolling by larvae carrying *ppk1.9-GAL4* alone ($n=40$) or *UAS-ChR2::eYFP* alone ($n=77$). (I,J) Dendritic trees of control and Lola knockdown ddaC cells visualized with mCD8::GFP. (K,L) Quantifications comparing controls ($n=10$) with *lola* RNAi ($n=10$). (K) Sholl profiles of dendrite density as a function of distance from the cell soma. (L) Morphometric properties of analyzed cells. Scale bars: 100 µm in A-D″,I,J; 40 µm in F,G.

Development (2014) doi:10.1242/dev.099655

arbors of the class IV da neuron ddaC. Although control ddaC neurons exhibited normal morphology and branching of their large radial arbors (Fig. 1I), *lola* RNAi neurons had fewer branches (Fig. 1J,K), their average total arbor length was reduced to 64.5% of controls (Fig. 1L), and there was reduced area of the field covered by dendritic branches (Fig. 1L). In addition, thin dendrites often proliferated in the proximal region of the arbor close to the cell soma (Fig. 1I,J). We used Sholl analysis (Sholl, 1953) to plot the density profiles of branches as a function of distance from the cell soma (Fig. 1K), and determined the peak of maximum branch density (critical value) and its corresponding radius (critical radius) (Ristanović et al., 2006). Both were dramatically reduced by *lola* RNAi (Fig. 1L), with the critical value reduced to 61.0% of controls and critical radius reduced by nearly half, from 203.5 to 113.8 µm. Thus, Lola promotes the appropriate number and positions of branches along the proximal-distal axis of dendritic arbors.

To test whether Lola function in dendrite morphogenesis was cell-autonomous, we used the MARCM (mosaic analysis with a repressible cell marker) technique (Lee and Luo, 1999) to selectively visualize single da neurons that were homozygous for *lola* mutations. We focused on two independent *lola* mutant alleles: the $lola^{ore76}$ null; and $lola^{5D2}$, a strong hypomorph (Giniger et al., 1994; Spletter et al., 2007). Although control MARCM clones exhibited normal morphology and branching (Fig. 2A), ddaC neurons mutant for either allele resembled *lola* RNAi in having far fewer branches (Fig. 2B,C), reduced total arbor length (Fig. 2D) and dendritic field (Fig. 2E), and numerous thin, ectopic dendrites near the cell soma (Fig. 2B,C). From Sholl density profiles (Fig. 2F), both critical value and critical radius were also dramatically reduced (Fig. 2G,H). Together, these results confirm that Lola controls branch number and position cell-autonomously in post-mitotic neurons. In addition, they validate both the specificity and effectiveness of the RNAi line we used to knock down *lola*.

We then examined class I da neurons, which have the smallest and simplest dendritic arbors. Compared with control MARCM clones (Fig. 2I), *lola* MARCM clones for ddaE had reduced growth of major dendritic branches (Fig. 2J,K), and reduced total arbor length (Fig. 2L). There was also a proliferation of abnormal, short branches (<10 µm), usually near the cell soma (Fig. 2J′,K′,M). Similar observations were made for ddaD, another class I da neuron (supplementary material Fig. S2). In MARCM analyses for the class II neuron ddaB, and the class III neuron ddaF, *lola* mutations caused reduced total arbor length but no inappropriate branching patterns (supplementary material Fig. S3).

In summary, loss of *lola* reduced the total lengths of dendritic arbors in da neurons. In classes IV and I it also caused inappropriate arrangements of branches, with the appearance of thin, abnormal branches near the cell soma of class IV da neurons, and short ectopic branches in class I da neurons.

Distinct Lola isoforms are required to shape da neuron dendrites

At least 19 isoforms of Lola are thought to be generated by alternative mRNA splicing (Goeke et al., 2003; Ohsako et al., 2003). To explore the contribution of Lola isoforms to dendrite morphogenesis, we examined MARCM clones for the mutations $lola^{orc4}$, which affects only Lola isoform K, and $lola^{orel19}$ (isoform L only) (Goeke et al., 2003). In class IV da neurons, both caused dendritic defects that resembled the null *lola* phenotype because they reduced arbor length and complexity, but were less severe and did not affect dendritic field or critical radius (supplementary material Fig. S4). In class I da neurons, arbor length was reduced, but there was no proliferation of short branches (supplementary material Fig. S4). Thus, the K and L isoforms are indeed important for dendrite morphogenesis, but other isoforms may be involved

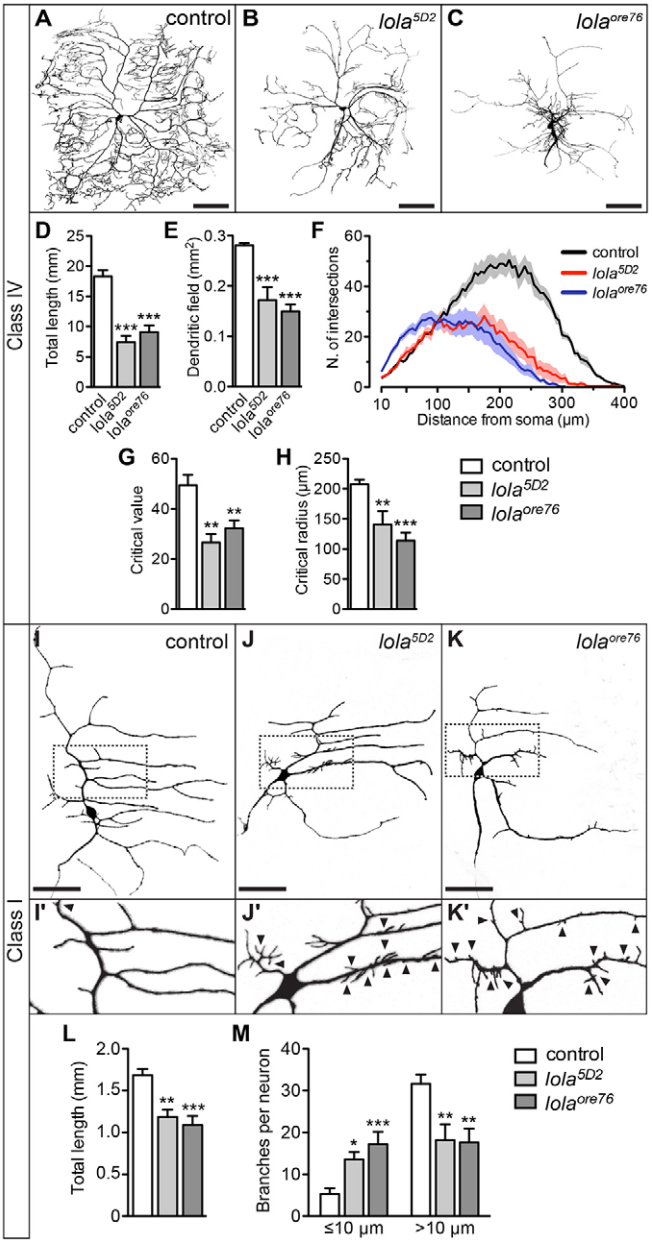

Fig. 2. Lola cell-autonomously controls the number, growth and distribution of dendrite branches. (A-H) Class IV ddaC neurons. MARCM clones in controls (A), $lola^{5D2}$ (B) and $lola^{ore76}$ (C). (D-H) Quantifications comparing control (n=12), $lola^{5D2}$ (n=12) and $lola^{ore76}$ (n=7) clones. (D) Total arbor length (ANOVA, $F_{2,28}$=29.50, P<0.0001). (E) Area of dendritic field (ANOVA, $F_{2,28}$=28.58, P<0.0001). (F-H) Sholl analysis. (F) Sholl profiles. (G) Critical value (ANOVA, $F_{2,25}$=8.360, P=0.0017). (H) Critical radius ($F_{2,25}$=19.68, P<0.0001). (I-M) Class I ddaE neurons. MARCM clones in controls (I), $lola^{5D2}$ (J) and $lola^{ore76}$ (K). Dotted boxes enlarged in I′,J′,K′ depicting numerous short branches in *lola* mutants (arrowheads). (L,M) Quantifications comparing control (n=9), $lola^{5D2}$ (n=5) and $lola^{ore76}$ (n=5) clones. (L) Total arbor length (ANOVA, $F_{2,16}$=14.02, P=0.0003). (M) Branch number per neuron below a 10 µm threshold (ANOVA, $F_{2,16}$=11.39, P=0.0007) or above ($F_{2,16}$=8.263, P=0.0034). Scale bars: 100 µm in A-C; 50 µm in I-K.

Development (2014) doi:10.1242/dev.099655

also. As neither could account for the complete null phenotype, we conclude that isoform diversity is an important aspect of *lola* function in da neurons.

Lola limits formation of F-actin-rich branches

Intrigued by the inappropriate branching patterns caused by loss of *lola*, we focused on class IV and class I da neurons to explore how Lola regulates the cytoskeleton. We labeled MTs or F-actin in da neurons where the loss of Lola promoted thin branches in bushy proximal arbors (class IV) or spiky ectopic branches (class I). In *lola* MARCM clones (supplementary material Fig. S5), or *lola* RNAi (Fig. 3A-B″,E-F″), these abnormal branches lacked labeling for Futsch, a neuron-specific marker of stabilized MTs (Fig. 3B′,F′,I). Instead, these branches labeled strongly with the F-actin reporter Lifeact::Ruby (Hatan et al., 2011) (Fig. 3D′,H′,I).

We also performed time-lapse imaging of class IV or class I da neurons of controls and *lola* RNAi animals at L3 (supplementary material Movies 1, 2). Consistent with the abundance of F-actin rich branches and their potential for increased motility, the number of dynamic terminal branches on *lola* RNAi neurons increased nearly threefold compared with age-matched controls (supplementary material Fig. S6).

Lola promotes the expression of Cut and Knot

We predicted that Lola shapes dendritic arbors by up- or downregulating specific target genes, and two candidates are the transcription factors Cut and Knot. Cut is a homeodomain protein required for dendrite arborization in da neurons of classes II, III and IV (Grueber et al., 2003), and Lola has been shown to regulate Cut expression and function in the developing wing (Krupp et al., 2005). Knot is a Collier/Olf1/EBF protein that promotes dendrite outgrowth and branching in class IV da neurons (Hattori et al., 2007; Jinushi-Nakao et al., 2007; Crozatier and Vincent, 2008). Using *lola* RNAi in class IV da neurons, we found that Lola promotes the expression of both Cut and Knot, as the normalized immunofluorescence for these proteins within nuclei of ddaC neurons was reduced to 48.3% and 57.0% of controls, respectively (Fig. 3J). Thus, Lola could influence how Cut and Knot control dendrite growth and branching in class IV da neurons. However, neither *cut* nor *knot* mutations cause a proliferation of F-actin rich proximal dendrites as we have

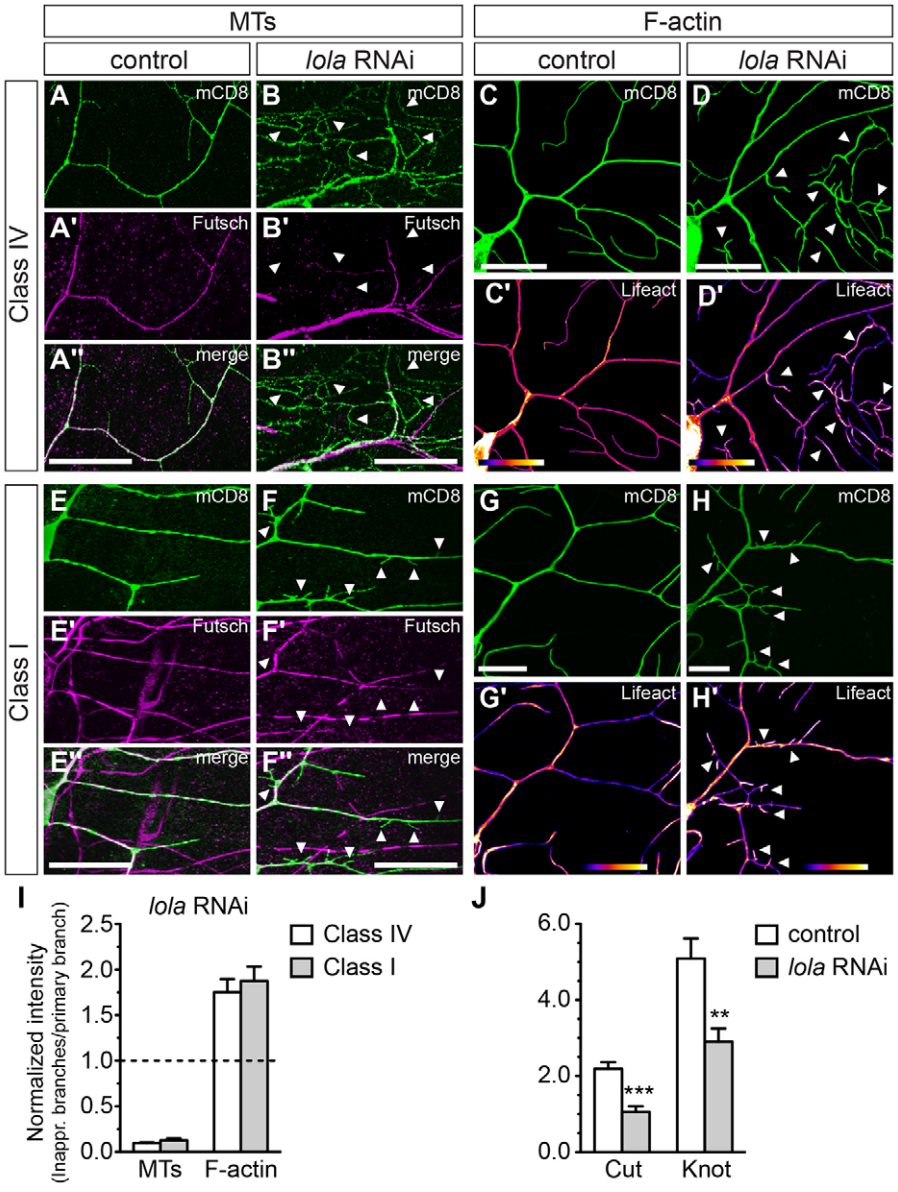

Fig. 3. Lola limits the appearance of inappropriate actin-rich branches. (A-B″) Class IV ddaC neurons (*ppk1.9-GAL4*) imaged for mCD8::GFP (using anti-GFP, green) and for anti-Futsch (magenta). Overlays in A″ and B″. *lola* RNAi induces numerous thin branches near the cell soma (arrowheads) that lack MTs (Futsch). (C-D′) Class IV ddaC neurons imaged for mCD8::GFP (green) and the F-actin reporter Lifeact-Ruby (C′,D′, pseudo-colored with a warmer hue indicating higher signal intensity). Thin branches near the cell soma in *lola* RNAi (arrowheads) are strongly labeled for Lifeact::Ruby. (E-F″) Class I ddaE neurons ($GAL4^{221}$) labeled for mCD8::GFP (anti-GFP, green) and anti-Futsch (magenta). Overlays in E″ and F″. Arrrowheads indicate that RNAi-induced short, spiky branches lack MTs (Futsch). (G-H′) Class I ddaE neurons imaged for mCD8::GFP (green) and Lifeact::Ruby. Short ectopic branches (arrowheads) in *lola* RNAi are intensely positive for F-actin. (I) Quantification of Futsch (MTs) and Lifeact::Ruby (F-actin) in inappropriate branches [i.e. thin (class IV) or short (class I)], relative to primary dendrites nearby, which were normalized to 1. (J) Lola knockdown in ddaC (*ppk1.9-GAL4*) reduces Cut and Knot immunoreactivity in cells labeled with CD4-tdTomato (*t*-test; Cut, $P<0.0001$; Knot, $P=0.0030$; $n=16$ per genotype). Scale bars: 100 µm in A-F″; 25 µm in C-D′; 50 µm in G-H′.

Development (2014) doi:10.1242/dev.099655

found for *lola* (Grueber et al., 2003; Jinushi-Nakao et al., 2007). Therefore, we sought alternative factors regulated by Lola that have the capacity to influence the dendritic F-actin cytoskeleton directly.

Lola limits expression of Spir

We considered the actin-nucleation factor Spir to be a candidate Lola effector because microarray and RT-qPCR assays demonstrated the *spire* (*spir*) gene to be upregulated threefold in *lola*^{ore76}-null mutant embryos relative to controls (Gates et al., 2011). The longest Spir isoform (SpirA) contains a KIND domain, four WH2 domains that bind actin monomers and promote F-actin nucleation (Wellington et al., 1999; Quinlan et al., 2005), as well as a SPIR-box and an mFYVE domain (Kerkhoff et al., 2001) (Fig. 4A). Expression of *spir* transcripts has been observed in the PNS and central nervous system (CNS) of *Drosophila* embryos (Gates et al., 2011), but Lola is expressed more broadly (Fig. 1A). The microarray and RT-qPCR assays were consistent with the idea that Lola represses expression of *spir* (Gates et al., 2011), but we wondered whether Lola regulates *spir* expression specifically within neurons, whether Spir is expressed in the dendrites of da neurons and functions in their arborization, and whether Lola controls dendrite morphogenesis through *spir*.

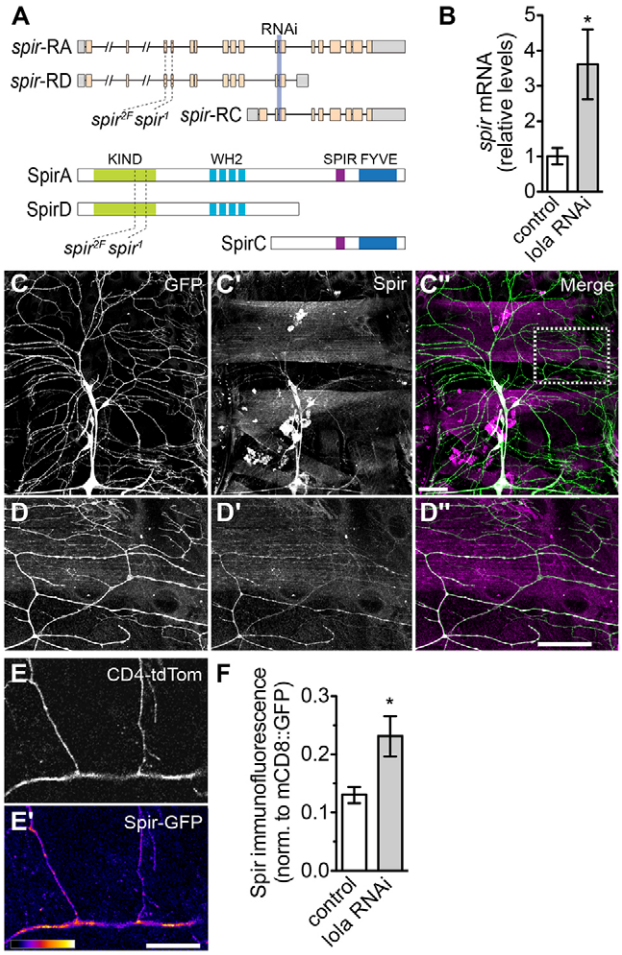

Fig. 4. Spir is expressed in dendrites of da neurons and limited by Lola. (A) *spir* transcripts with intron/exon structures (upper) and Spir polypeptides (lower). *spir*^{2F} and *spir*^{1} mutations map to the KIND domain. Sequence targeted by RNAi is indicated, and present in all isoforms. (B) RT-qPCR showing relative *spir* mRNA levels in controls versus *lola* RNAi, both normalized to those of GAPDH (*t*-test, P=0.0458). (C) Dorsal cluster of da neurons of control L3 larva labeled by GAL4$^{109(2)80}$-driven UAS-mCD8::GFP. (C′) Anti-Spir labeling showing expression in all da neurons. Overlay is shown in C″. (D-D″) Higher magnification of area outlined in C″, showing Spir expressed within dendrites of da neurons (ddaE and ddaC shown). (E,E′) *ppk1.9-GAL4* was used to simultaneously express CD4-tdTomato and Spir-GFP (pseudo-colored heat map of intensity). (F) Lola knockdown increases Spir immunofluorescence in da neurons (normalized to mCD8::GFP) (*t*-test, P=0.0255; controls, n=10; *lola* RNAi n=14). Scale bars: 50 µm.

To test whether Lola specifically regulates *spir* expression within neurons, we used nSyb-Gal4 to knock down Lola in postmitotic neurons of CNS and PNS, including da neurons. We collected L1 larvae to sample a stage of continuing dendrite growth and branching, and used RT-qPCR to assess the relative levels of *spir* mRNA expression compared with controls. Lola knockdown in only postmitotic neurons caused a 3.6-fold increase in *spir* mRNA levels (Fig. 4B), raising the possibility that one way in which Lola could control development of neuronal dendrites is through balanced control of intrinsic Spir levels.

Spir is expressed in the dendrites of da neurons and promotes F-actin there

Using immunohistochemistry, Spir protein was observed in all the da neurons within the dorsal cluster of larval PNS neurons (Fig. 4C′), plus a limited number of cells nearby. Spir was expressed in the dendrites of da neurons, and also in their cell bodies and axons (Fig. 4C′,D′). With a low-expressing Spir-GFP fusion protein to report the subcellular distribution of Spir, we noted Spir-GFP along branches and at branch points (Fig. 4E,E′). To test whether Lola regulates Spir expression in da neurons, we measured normalized immunofluorescence for the Spir protein in classes I and IV da neurons and found that Lola knockdown caused an average 1.8-fold increase of Spir (Fig. 4F).

Spir expression within dendrites suggested that Spir could locally modify F-actin levels and influence dendrite branching directly, and so we sought to examine the effects of *spir* loss-of-function on these processes. We used RNAi to specifically knock down endogenous Spir levels in class IV da neurons, targeting all *spir* isoforms via a common sequence (Fig. 4A). This reduced Spir expression in class IV da neurons, which at once confirmed the specificity of the Spir antibody and the effectiveness of Spir knockdown (Fig. 5A,B). Consistent with a role in nucleating F-actin within dendritic arbors, RNAi knockdown of Spir reduced the normalized intensity of the F-actin reporter Lifeact-GFP to 65.1% of controls (Fig. 5C-E).

Spir promotes dendrite branches and limits their distribution to appropriate positions along the proximal-distal axis of the arbor

Spir knockdown affected dendrite branching in class IV da neurons in two ways (Fig. 5F-K). First, it reduced the total number of branch ends per neuron to 76.9% of controls and total arbor length to 83.1% of controls (Fig. 5I). Second, we noted that in Spir knockdown there was an accumulation of small branches at the most distal reaches of the arbor (Fig. 5G), consistent with the fact that dendritic field was not reduced (Fig. 5I). Sholl analysis (Fig. 5H) confirmed that there was a distal shift in the critical radius by an average of 24.6 µm compared with controls (Fig. 5I). A modified Strahler analysis (Strahler, 1957) found that Spir knockdown preferentially reduced the numbers of terminal branches (Strahler order 1), with consistently fewer branches in each of the remaining orders (Fig. 5J). This agreed with the loss of proximal branches, as revealed in the Sholl profile (Fig. 5H). We also varied the approach of Schoenen (Schoenen, 1982) to calculate the ratios of branch numbers between successive Strahler orders (Fig. 5K). Spir

Development (2014) doi:10.1242/dev.099655

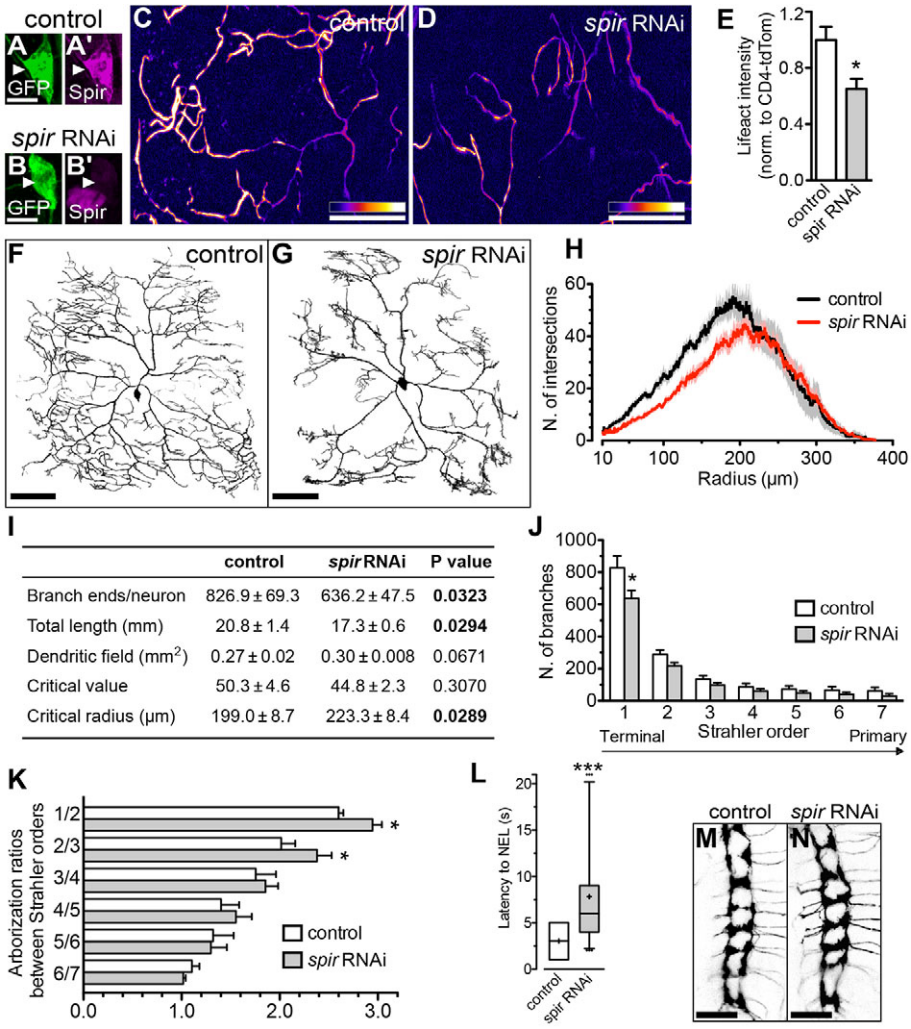

Fig. 5. Spir promotes F-actin and is required for correct dendrite arborization and positioning. (A-B′) Compared with controls, *spir* RNAi abolishes Spir protein in class IV neuron ddaC (arrowheads, *ppk1.9-GAL4*). (C,D) Pseudo-colored heatmap images of *ppk1.9-GAL4*-driven Lifeact::GFP intensity in distal dendrites of ddaC neurons. (E) Quantification of Lifeact::GFP intensities normalized to those of CD4-tdTomato (*t*-test, P=0.0355; controls, n=6; *spir* RNAi, n=8). (F,G) Control and *spir* RNAi class IV ddaC neurons, visualized by *ppk1.9-GAL4* driving *UAS-CD4-tdTomato*. (H-K) Quantifications of dendrite parameters comparing controls (n=13) with *spir* RNAi (n=11). (H) Sholl profiles. (I) Morphometry of ddaC arbors (mean±standard error). (J) Number of branches at each Strahler order. *spir* RNAi significantly reduces the number of terminal branches (Strahler order 1, two-way ANOVA, P<0.0001), although there are consistently fewer branches of all orders. (K) Ratios of the numbers of branches between consecutive Strahler orders reveal that *spir* RNAi increases arborization of terminal and penultimate branches (two-way ANOVA, P<0.0001). (L) Boxplot of latencies to initiate NEL from probe at 45°C (*t*-test, P<0.0001; controls, n=19; *spir* RNAi, n=31). (M,N) Terminals of *ppk-CD4::tdTomato*-labeled axons appear unaffected by *spir* RNAi. Scale bars: 25 μm in A-B′; 50 μm in C,D; 100 μm in F,G; 40 μm in M,N.

knockdown increased the degree of ramification in only terminal and penultimate Strahler orders (Fig. 5K), reflected particularly in the distal reaches of these radial arbors. These results indicate a central role for Spir in determining branch number and distribution in complex dendrites, likely via promoting F-actin within branches (Fig. 5C-E).

We tested whether selective Spir RNAi knockdown in class IV neurons compromised nocifensive responses. Relative to controls (mean latency 3.0 seconds), loss of Spir delayed larval responses considerably (mean 7.8 seconds), with 9.7% of larvae failing to respond within 20 seconds (Fig. 5L). The axon terminals of these neurons within the VNC appeared intact (Fig. 5M,N).

Lola controls dendrite morphogenesis through Spir

Our results pointed to a role for Spir-dependent F-actin synthesis in positioning dendritic branches along the proximal-distal axis of the arbor, and so we surmised that *lola* mutations could fail to control the levels of Spir, leading to deregulation of actin filament assembly and the formation of inappropriate F-actin-rich dendrite branches in da neurons. Therefore, we predicted that reduced gene dose of *spir* would suppress the effects of *lola* loss of function in dendrites. We tested this prediction using two *spir* alleles ($spir^{2F}$ and $spir^{1}$), both of which truncate Spir within the KIND domain and therefore lack the WH2 domains that are crucial for actin nucleation (Fig. 4A). Both *spir* alleles had the same effects. In class IV da neurons, the thin, inappropriate branches induced by *lola* RNAi were indeed suppressed in *spir* heterozygotes compared with controls (Fig. 6A-D). In addition, outgrowth of major branches was partially restored, as reflected by increased dendritic field (Fig. 6F), and critical radius was shifted distally toward its normal position from the cell soma (Fig. 6G,I). Neither total arbor length nor critical value was restored to any degree in *spir* heterozygotes (Fig. 6E,H). Remarkably, reduced *spir* gene dose also led to functional recovery from the nocifensive behavioral deficit caused by *lola* RNAi in class IV da neurons (Fig. 6J), highlighting the importance of the Lola-Spir pathway for neuronal function. In class I da neurons where *lola* RNAi ($GAL4^{221}$) induced the short ectopic branches that are characteristic of *lola* mutations (Fig. 6K,L), these ectopic branches were suppressed by reduced *spir* gene dose (Fig. 6K-P).

Our data support a model in which Lola represses Spir within da neurons to levels that provide a balanced degree of local F-actin synthesis within dendrites (Fig. 7A). Spir specifically regulates the positioning of branches within arbors, whereas other Lola effectors (perhaps including Cut and Knot) are likely to have a more profound impact on branch number and total arbor length. To understand how Spir influences the positioning of branches within arbors, we generated branch density profiles for class IV da neurons (Fig. 7B). We averaged these profiles for each of the genotypes that we tested (Fig. 7C), and found an inverse correlation between critical radius and the relative levels of Spir that we determined experimentally or

Development (2014) doi:10.1242/dev.099655

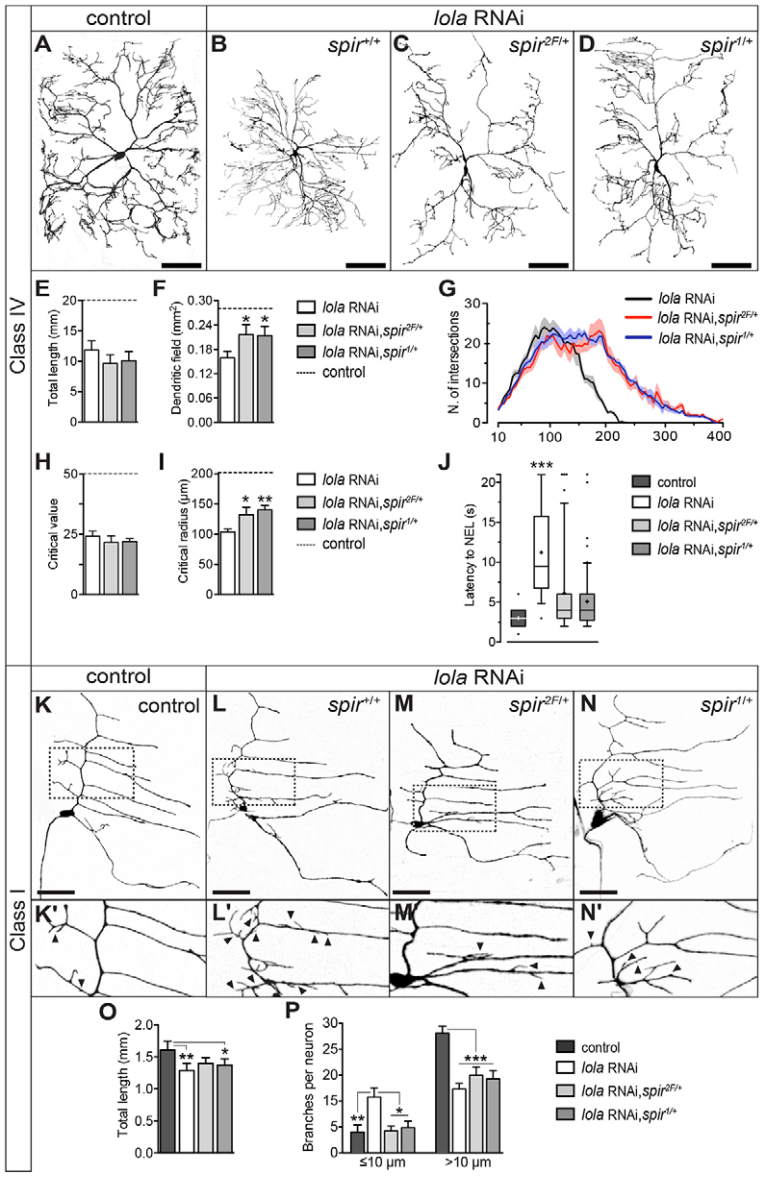

Fig. 6. Suppression of *lola* loss of function by reduced *spir* gene dose. (A-J) Class IV ddaC neurons (*ppk1.9-GAL4*). *lola* RNAi reduces arbor size and increases branch density near the soma (B). These effects are suppressed in $spir^{2F}$ (C) or $spir^{1}$ (D) heterozygotes. (E-I) ddaC quantifications comparing *lola* RNAi (n=11) with *lola* RNAi, $spir^{2F/+}$ (n=6) or *lola* RNAi, $spir^{1/+}$ (n=7). (G) Sholl analysis. (E) Reduced *spir* dose does not restore total arbor length (ANOVA, $F_{2,21}$=0.5703, P=0.5743), or (H) critical value (ANOVA, $F_{2,21}$=0.3737, P=0.6931) to *lola* knockdown neurons, but it does restore (F) dendritic field (ANOVA, $F_{2,21}$=3.300, P=0.0409) and suppress the appearance of inappropriate proximal dendrites, leading to a distal shift of (I) critical radius (ANOVA, $F_{2,21}$=3.896, *P=0.0364). For reference, dashed lines indicate average values for control neurons quantified in Fig. 1I-L. (J) Boxplot of latencies to initiate NEL (45°C). *spir* heterozygosity restores behavioral performance to control levels [ANOVA, $F_{3,126}$=10.42, P<0.0001 (controls, n=21; *lola* RNAi, n=18; *lola* RNAi,$spir^{2F/+}$, n=50; *lola* RNAi,$spir^{1/+}$, n=43]. (K-P) Class I ddaE neurons ($GAL4^{221}$). *lola* RNAi induces short (<10 µm) branches (arrowheads) (L,L′), which are suppressed when heterozygous for $spir^{2F}$ (M,M′) or $spir^{1}$ (N,N′). (O,P) Quantifications in class I ddaE neurons comparing controls (n=7) and *lola* RNAi (n=8) with *lola* RNAi, $spir^{2F/+}$ (n=7) or *lola* RNAi, $spir^{1/+}$ (n=7). (O) Total arbor length (ANOVA $F_{3,25}$=0.6.605, P=0.0019). (P) Number of branches shorter than 10 µm (ANOVA $F_{3,25}$=5.361, P=0.0055) or longer than 10 µm (ANOVA $F_{3,25}$=17.14, P<0.0001). Scale bars: 100 µm.

inferred from genetic approaches. We propose that the Lola-Spir pathway generates a balance of F-actin that determines where the density of branches is greatest along the proximal-distal axis of dendritic arbors (Fig. 7D).

DISCUSSION

We discovered that dendrites in *Drosophila* are sculpted by a molecular pathway controlled by the transcription factor Lola. Superficially the *lola* phenotype resembled that of *dynein* in that both mutations cause branches to be mis-positioned closer to the cell soma (Satoh et al., 2008; Zheng et al., 2008). However, in *dynein*, these branches have MTs whereas in *lola* they are F-actin rich, suggesting distinct mechanisms. Instead, we found that Lola regulates levels of the actin nucleator Spir, which are crucial for the abundance of F-actin in developing dendritic arbors and for proper positioning of branches. Lola acts within neurons to regulate Spir expression at the level of transcription, though additional research will be needed to determine whether this regulation is direct and which of the 19 or more Lola isoforms are relevant. Perturbations of the Lola-Spir pathway impair sensory neuron function and disrupt innate avoidance behaviors to noxious stimuli. Although Lola and Spir may affect additional unknown aspects of neuronal physiology, we propose that the Lola-Spir pathway is crucial for neural circuit function, at least in part because it provides balanced control of the F-actin cytoskeleton and thereby contributes to the spatial arrangement of branches within dendritic trees.

Lola is expressed in all da neurons, and in every class it promotes dendrite growth. However, branching defects are found only in classes I and IV, which could reflect context-dependent use of Lola, or cell-type specific thresholds for its activity. Another BTB-Zn-finger transcription factor, Abrupt, is selectively expressed in class I da neurons, where it limits higher-order branching and restricts total arbor size (Li et al., 2004; Sugimura et al., 2004), demonstrating how different members of this interesting protein family shape class I arbors via distinct influences on dendrite branching and outgrowth. Additional transcription factors belonging to other families undoubtedly collaborate with BTB-Zn-finger proteins for class-specific patterns of arborization. These include Cut and Knot, which control dendrite growth and branching in class IV da neurons. Cut and Knot have little or no influence on the

Development (2014) doi:10.1242/dev.099655

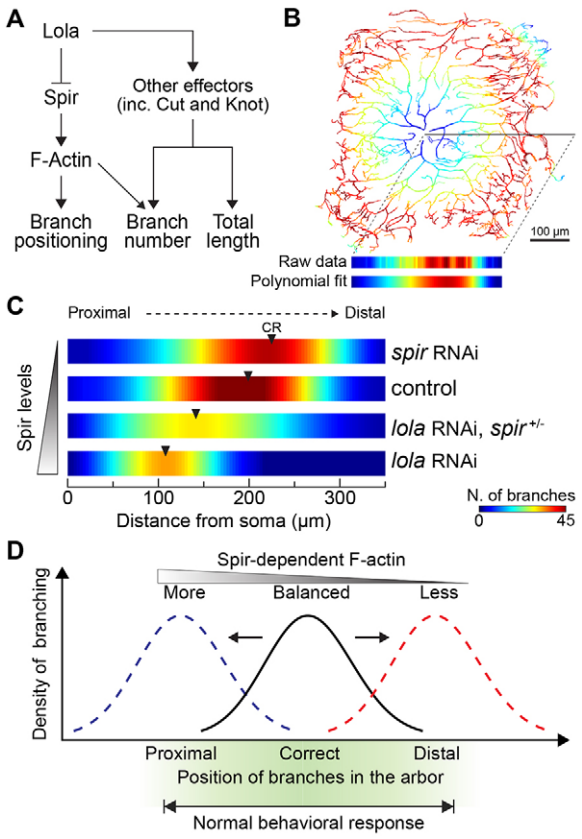

Fig. 7. The Lola-Spir pathway and dendrite morphogenesis. (A) Genetic model for Lola in dendrite positioning, branch number and total arbor length. (B) Class IV ddaC neuron, showing a pseudo-colored heat-map of Sholl branch density. Measured values (raw data) can be fitted to a polynomial function to better discern trends in branch density. (C) Sholl profiles for individual neurons were pooled for each genotype and the average density profile fitted to a polynomial function. Average critical radius (CR) is shifted proximally by *lola* loss of function, but CR is partially restored in *spir* heterozygotes (data pooled from $spir^{1}$ and $spir^{2F}$ mutants). By contrast, *spir* loss of function causes the average CR to be positioned distal to that of controls. (D) Model for how Spir-induced F-actin correlates with the positioning of branches along the proximal-distal axis of the arbor.

expression of one another and are thought to act independently (Hattori et al., 2007; Jinushi-Nakao et al., 2007; Crozatier and Vincent, 2008), but as Lola promotes expression of both, perhaps it can coordinate and fine-tune their activities. To date, the effectors of Cut and Knot that directly remodel the dendritic cytoskeleton are unknown. Knot may promote expression of the MT-severing protein Spastin (Jinushi-Nakao et al., 2007; Ye et al., 2011), and Cut is thought to promote F-actin because high Cut levels coincide with class III morphology and the appearance of F-actin-rich spiked protrusions (Grueber et al., 2003; Jinushi-Nakao et al., 2007). As Lola promotes Cut expression, but limits Spir to prevent the appearance of inappropriate F-actin rich branches, we propose that Lola regulates Spir via a pathway that does not include Cut (Fig. 7A).

Spir levels correlate with the placement of branches within dendritic arbors: elevated Spir promotes branches near the cell soma whereas reduced Spir shifts branch density distally. As perturbations of Lola or Spir do not overtly affect axon guidance in class IV neurons, and as recovery from the nocifensive behavioral deficit in *lola* RNAi animals can occur without restoration of arbor complexity (critical value) or total arbor length, we propose that these shifts in the proximal-distal arrangement of dendritic branches can severely impact neural circuits and impair behavioral performance (Fig. 7D).

Our data are consistent with the idea that Spir nucleates *de novo* actin filaments in dendrites via its WH2 and KIND domains, but Spir activity could be more complex as Spir can also sequester, sever and depolymerize F-actin *in vitro* (Chen et al., 2012). We think it is likely that Spir contributes to specific subcellular F-actin pools or structures that promote the probability of dendrite branching at their correct positions within arbors, perhaps acting in concert with other nucleators such as the Arp2/3 complex and formins. Such F-actin could be dynamically engaged with MTs in the dendritic cytoskeleton, as occurs in the cytoplasm of *Drosophila* oocytes where Spir cooperates with the formin Cappuccino in the assembly of an F-actin structure that prevents premature rearrangement of MTs (Rosales-Nieves et al., 2006; Bosch et al., 2007; Dahlgaard et al., 2007). Notably, Spir overexpression in either class IV or class I da neurons, with or without simultaneous overexpression of Cappuccino, was insufficient to induce any overt effects (data not shown). Thus, additional factors are likely to cooperate with Spir to influence dendrite morphogenesis.

Whether Spir-like proteins are involved in dendrite morphogenesis in mammals has not been reported, but it is intriguing that murine orthologs of Spir (Spir1 and Spir2) are expressed primarily in the developing CNS and adult brain (Schumacher et al., 2004; Pleiser et al., 2010). Spir proteins belong to a family of actin nucleators that includes Cordon-bleu (Cobl) and Junction-mediating and regulatory protein (JMY). Knockdown of Cobl reduced dendrite branching complexity in cultures of rat hippocampal neurons (Ahuja et al., 2007), and in Purkinje neurons in organotypic slices of mouse cerebellum (Haag et al., 2012), while JMY knockdown in mouse neuroblastoma cells enhanced neurite outgrowth (Firat-Karalar et al., 2011). Future experiments will determine whether and how Cobl, JMY and Spir proteins influence dendrite arborization in the mammalian brain. In this regard, our research in *Drosophila* raises the exciting possibility that balanced regulation of Spir and related actin nucleators is a conserved mechanism for shaping architectures of dendritic trees.

MATERIALS AND METHODS

Fly stocks and genetics

Drosophila stocks were obtained from Bloomington Stock Center ($spir^{2F}$, $spir^{1}$, *UAS-spir::GFP.RD[30]*, *UAS-capu*, *UAS-Lifeact::GFP*, *UAS-Lifeact::Ruby*, *UAS-syt::eGFP*, *UAS-n-syb::eGFP*, $GAL4^{109(2)80}$ and $GAL4^{221}$); from the Vienna *Drosophila* Resource Center [UAS-RNAi for *lola* (transformant ID 101925), UAS-RNAi for *spir* (transformant ID 107335), UAS-Dcr2 (Dietzl et al., 2007); and from published sources (*ppk-CD4::tdTomato*, *ppk1.9-GAL4*, *UAS-ChR2::eYFP[C]* and $tutl^{GAL4}$).

For *lola* MARCM, virgin females of the stock $elav^{C155}$*-GAL4,UAS-mCD8::GFP,hs-FLP;FRTG13* (or *FRT42D),tub-GAL80* were crossed to males that were either $elav^{C155}$*-GAL4,UAS-mCD8::GFP,hs-FLP;FRTG13* (or *FRT42D*) or $elav^{C155}$*-GAL4,UAS-mCD8::GFP,hs-FLP;FRTG13,* $lola^{ore76}$ (or *FRT42D,* $lola^{5D2}$). Embryos were collected for 2 hours, incubated at 25°C for 2-3 hours, then heat-shocked at 38°C for 1 hour and raised at 25°C until analyzed at L3.

For all RNAi experiments, control animals carried the Gal4 driver (*ppk1.9-GAL4* or $GAL4^{221}$), *UAS-Dcr2* and a fluorescent reporter (i.e. *UAS-mCD8::GFP*, *UAS-Lifeact::Ruby*, *ppk-CD4::tdTomato*, *UAS-ChR2::eYFP*, etc.). For experimental groups, we added a single copy of the RNAi-inducing construct. For RT-qPCR experiments, we used nSyb-GAL4, a postmitotic pan-neuronal driver line created by Dr Julie Simpson, for which we used 2nd chromosome insertions generated by Dr Stefan Thor.

Immunohistochemistry

Larvae (L3) were dissected and prepared for immunohistochemistry as described previously (Ou et al., 2008). Primary antibodies used were: rabbit anti-Lola (1:200) (Giniger et al., 1994); mouse anti-Spir (1:100) (Liu et al., 2009); mouse anti-Futsch (1:300; mAb 22C10, DSHB; chicken anti-GFP (1:1000; Aves Labs); mouse anti-Cut (1:50; mAb 2B10, DSHB); and guinea pig anti-Knot (1:1000) (Baumgardt et al., 2007). Secondary antibodies used were: Alexa Fluor 488/568/647 (1:500; Molecular Probes).

To quantify Cut and Knot immunofluorescence, average intensity was measured within a region of interest (ROI) encompassing each cell soma, and normalized to that of *ppk-CD4::tdTomato*. Similarly, Spir and Lola immunofluorescence was quantified in ddaE (*Gal4*^{221}) and ddaC neurons (*ppk1.9-Gal4*) labeled with mCD8::GFP. Mean intensity of tdTomato or GFP was equivalent between controls and RNAi groups (data not shown).

Imaging

For imaging native fluorescence (mCD8-GFP, CD4-tdTomato, CD4-GFP, spir-GFP, Lifeact-GFP or Lifeact-Ruby), larvae (L3) were prepared as described previously (Ou et al., 2008). The Lifeact peptide does not affect actin polymerization and is unique to yeast (Riedl et al., 2008). Lifeact reporters labeled da neuron dendrites with signal that was often discontinuous and of variable intensity, consistent with previous reports for actin-GFP and GMA-GFP (Andersen et al., 2005; Medina et al., 2006; Jinushi-Nakao et al., 2007; Lee et al., 2011; Nagel et al., 2012), though GMA-GFP seems enriched at branch termini.

Images were acquired with a Yokogawa spinning disk system (Perkin-Elmer) on an Eclipse TE2000-U microscope (Nikon) or with a Fluoview FV1000 confocal laser scanning microscope (Olympus) and processed using Fiji (Schindelin et al., 2012; Schneider et al., 2012). When required, stacks were registered (Thévenaz et al., 1998) and stitched together (Preibisch et al., 2009). For time-lapse, L3 larvae in halocarbon oil were immobilized by gentle pressure in an imaging chamber (RC-30WA, Warner Instruments). Image stacks were acquired every 5 minutes for 1 hour, and each time-series was registered using a descriptor-based approach (Preibisch et al., 2010). Branch ends were tracked using MTrackJ (Meijering et al., 2012) and classified as described previously (Stewart et al., 2012) using routines described previously (Ferreira et al., 2010).

To measure Lifeact::Ruby and Futsch within dendrites (Fig. 3A-I), image fields (three or four per neuron) were acquired of arbors near the cell soma, and topological skeletons of GFP-labeled dendrites created as described below. Skeletons were converted to ROIs, tracing branches along their center lines. Average intensities were retrieved and values for inappropriate branches (RNAi-induced) were normalized to those of neighboring primary dendrites.

To quantify Lifeact::GFP in control and *spir* RNAi arbors (Fig. 5C-E), we aligned image fields containing tdTomato-labeled dendrites with denticle belts at the anterior segment boundary, then acquired the Lifeact::GFP signal, quantified it on skeletonized ROIs (as above), and normalized to tdTomato.

Dendrite morphometry

Background was first subtracted from maximum-intensity projections (MIPs) of image stacks. Dendrites were segmented using a custom, semi-automated procedure based on adaptive thresholding. The resulting MIP mask (with axons cleared manually) was applied to the image stack to select fluorescence from dendritic arbors only. To measure branch lengths, dendrites were traced in three dimensions using Simple Neurite Tracer (Longair et al., 2011). For class I, a 10 µm cut-off for short branches was determined empirically: from nine control ddaE cells, terminal branches shorter than 10 µm occurred with a frequency of 9.8%. To automate analysis of class IV arbors, segmented images were converted to three-dimensional topological skeletons. From these were retrieved segment lengths, number of branch ends and positions of branch points (Arganda-Carreras et al., 2010; Doube et al., 2010). Dendritic field was the area of the smallest convex polygon containing the planar *z*-projected neuron, using Convex Hull Plus by G. Landini.

For Sholl analysis (Sholl, 1953), we developed a plug-in (http://fiji.sc/Sholl_Analysis) to implement a modified method (Ristanović et al., 2006) for accurate retrieval of descriptors of dendritic density from bitmap images. The Sholl profile of each neuron was fitted to an 8th degree polynomial, from which we determined the local maximum (critical value) and the distance at which it occurred (critical radius). For Strahler analysis (Strahler, 1957), we developed a script (http://fiji.sc/Strahler_Analysis) to parse skeletonized stacks by iteratively pruning terminal branches and counting branch number in each iteration.

Real-time quantitative PCR (RT-qPCR)

RNA and cDNA was isolated in three independent extractions from L1 larvae raised at 29°C (Qiagen). RT-qPCR used SYBR Green in a StepOnePlus system (Applied Biosystems), with GAPDH mRNA for normalization. Primers were (5′-3′): GAPDH (forward), CACTGCCG-AGGAGGTCAACTAC; GAPDH (reverse), ATGCTCAGGGTGATTG-CGTATGC; Spir (forward), AACACCCAAGCCACGAC; Spir (reverse), TGCTGATGCTGTTCTCATCG. The Spir primers amplified 149 bp spanning two exons common to all Spir isoforms.

Nocifensive escape locomotion

L3 larvae were tested for nociception with a custom-built heat probe (Babcock et al., 2009), using an external thermocouple to monitor the probe tip and calibrate the controller. Stimulus was delivered as described previously (Chattopadhyay et al., 2012), with each larva tested once. Nocifensive escape locomotion (NEL) latency was the time from probe contact until the larva initiated one complete evasive rotation. For larvae that did not respond to stimulation within 20 seconds, stimulus was terminated and a latency of 21 seconds was assigned (Caldwell and Tracey, 2010).

Optogenetics

L3 controls (*UAS-Dcr2;UAS-ChR-2::YFP;ppk1.9-GAL4*) and *lola* RNAi (*UAS-Dcr2;UAS-ChR-2::YFP,UAS-RNAi;ppk1.9-GAL4*) were tested in three trials as described previously (Honjo et al., 2012), but stimulated with a 470 nm LED driven by a 1000 mA power driver (Luxeon Star) coupled to a 3 mm optic fiber (Edmund Optics) outputting a radiant flux of 10-15 mW and positioned 5 mm above larvae at a 40° angle.

Graphs and statistics

Bar graphs and tables of dendrite morphometry express data as mean ± standard error. Graphs of nocifensive behavior express data in box plots showing median (horizontal line), mean (+) and limits of the first and third quartiles. Whiskers depict the 10th and 90th percentiles, and outliers are marked by dots. Statistical analyses were carried out in Prism (GraphPad). Unless otherwise stated, data were tested for normal distribution (Shapiro-Wilk), and analyzed for statistical significance using two-tailed unpaired Student's *t*-tests (two groups only), or one-way ANOVA (multiple groups). ANOVA at $P<0.05$ was followed by Dunnett's post-hoc tests, and asterisks in graphs indicate the significance of *P*-values comparing indicated group with controls (*$P<0.05$; **$P<0.01$; ***$P<0.001$).

Acknowledgements

For flies/reagents, we thank Susan Parkhurst, Frieder Schoeck, Frank Schnorrer, Yuh-Nung Jan, Dan Tracey, Julie Simpson, Stefan Thor and stock centers in Bloomington, Vienna and Kyoto. Michael Gates and Fen-Biao Gao kindly shared results prior to publication. For helpful advice, we thank Yong Rao, Keith Murai, Charles Bourque, Ellis Cooper, Stefan Thor, Jean-Francois Cloutier, Todd Farmer and members of van Meyel lab.

Competing interests

The authors declare no competing financial interests.

Author contributions

T.F. and Y.O. conceived and performed experiments, and wrote the manuscript; S.L. performed experiments; E.G. and D.J.v.M. conceived experiments and wrote the manuscript.

Funding

Supported by grants to D.J.v.M. from the Canadian Institutes of Health Research, the Natural Sciences and Engineering Research Council of Canada, and the Canada Foundation for Innovation, and by grants to E.G. from the Intramural

Research Program of the National Institutes of Health, National Institute of Neurological Disorders and Stroke [Z01-NS003013]. Training/salary awards came from the Research Institute of McGill University Health Center (Y.O. and T.F.) and from the McGill Faculty of Medicine (Y.O. and D.J.v.M.). Deposited in PMC for release after 12 months.

Supplementary material

Supplementary material available online at
http://dev.biologists.org/lookup/suppl/doi:10.1242/dev.099655/-/DC1

References

Ahuja, R., Pinyol, R., Reichenbach, N., Custer, L., Klingensmith, J., Kessels, M. M. and Qualmann, B. (2007). Cordon-bleu is an actin nucleation factor and controls neuronal morphology. *Cell* **131**, 337-350.

Andersen, R., Li, Y., Resseguie, M. and Brenman, J. E. (2005). Calcium/calmodulin-dependent protein kinase II alters structural plasticity and cytoskeletal dynamics in Drosophila. *J. Neurosci.* **25**, 8878-8888.

Arganda-Carreras, I., Fernández-González, R., Muñoz-Barrutia, A. and Ortiz-De-Solorzano, C. (2010). 3D reconstruction of histological sections: Application to mammary gland tissue. *Microsc. Res. Tech.* **73**, 1019-1029.

Babcock, D. T., Landry, C. and Galko, M. J. (2009). Cytokine signaling mediates UV-induced nociceptive sensitization in Drosophila larvae. *Curr. Biol.* **19**, 799-806.

Baumgardt, M., Miguel-Aliaga, I., Karlsson, D., Ekman, H. and Thor, S. (2007). Specification of neuronal identities by feedforward combinatorial coding. *PLoS Biol.* **5**, e37.

Bosch, M., Le, K. H., Bugyi, B., Correia, J. J., Renault, L. and Carlier, M. F. (2007). Analysis of the function of Spire in actin assembly and its synergy with formin and profilin. *Mol. Cell* **28**, 555-568.

Caldwell, J. C. and Tracey, W. D., Jr (2010). Alternatives to mammalian pain models 2: using Drosophila to identify novel genes involved in nociception. *Methods Mol. Biol.* **617**, 19-29.

Chattopadhyay, A., Gilstrap, A. V. and Galko, M. J. (2012). Local and global methods of assessing thermal nociception in Drosophila larvae. *J. Vis. Exp.* **63**, e3837.

Chen, C. K., Sawaya, M. R., Phillips, M. L., Reisler, E. and Quinlan, M. E. (2012). Multiple forms of Spire-actin complexes and their functional consequences. *J. Biol. Chem.* **287**, 10684-10692.

Crowner, D., Madden, K., Goeke, S. and Giniger, E. (2002). Lola regulates midline crossing of CNS axons in Drosophila. *Development* **129**, 1317-1325.

Crozatier, M. and Vincent, A. (2008). Control of multidendritic neuron differentiation in Drosophila: the role of Collier. *Dev. Biol.* **315**, 232-242.

Dahlgaard, K., Raposo, A. A., Niccoli, T. and St Johnston, D. (2007). Capu and Spire assemble a cytoplasmic actin mesh that maintains microtubule organization in the Drosophila oocyte. *Dev. Cell* **13**, 539-553.

de la Torre-Ubieta, L. and Bonni, A. (2011). Transcriptional regulation of neuronal polarity and morphogenesis in the mammalian brain. *Neuron* **72**, 22-40.

Dietzl, G., Chen, D., Schnorrer, F., Su, K. C., Barinova, Y., Fellner, M., Gasser, B., Kinsey, K., Oppel, S., Scheiblauer, S. et al. (2007). A genome-wide transgenic RNAi library for conditional gene inactivation in Drosophila. *Nature* **448**, 151-156.

Doube, M., Kłosowski, M. M., Arganda-Carreras, I., Cordelières, F. P., Dougherty, R. P., Jackson, J. S., Schmid, B., Hutchinson, J. R. and Shefelbine, S. J. (2010). BoneJ: Free and extensible bone image analysis in ImageJ. *Bone* **47**, 1076-1079.

Ferreira, T. A., Iacono, L. L. and Gross, C. T. (2010). Serotonin receptor 1A modulates actin dynamics and restricts dendritic growth in hippocampal neurons. *Eur. J. Neurosci.* **32**, 18-26.

Firat-Karalar, E. N., Hsiue, P. P. and Welch, M. D. (2011). The actin nucleation factor JMY is a negative regulator of neuritogenesis. *Mol. Biol. Cell* **22**, 4563-4574.

Gao, F. B., Brenman, J. E., Jan, L. Y. and Jan, Y. N. (1999). Genes regulating dendritic outgrowth, branching, and routing in Drosophila. *Genes Dev.* **13**, 2549-2561.

Gates, M. A., Kannan, R. and Giniger, E. (2011). A genome-wide analysis reveals that the Drosophila transcription factor Lola promotes axon growth in part by suppressing expression of the actin nucleation factor Spire. *Neural Dev.* **6**, 37.

Giniger, E., Tietje, K., Jan, L. Y. and Jan, Y. N. (1994). lola encodes a putative transcription factor required for axon growth and guidance in Drosophila. *Development* **120**, 1385-1398.

Goeke, S., Greene, E. A., Grant, P. K., Gates, M. A., Crowner, D., Aigaki, T. and Giniger, E. (2003). Alternative splicing of lola generates 19 transcription factors controlling axon guidance in Drosophila. *Nat. Neurosci.* **6**, 917-924.

Grueber, W. B., Jan, L. Y. and Jan, Y. N. (2002). Tiling of the Drosophila epidermis by multidendritic sensory neurons. *Development* **129**, 2867-2878.

Grueber, W. B., Jan, L. Y. and Jan, Y. N. (2003). Different levels of the homeodomain protein cut regulate distinct dendrite branching patterns of Drosophila multidendritic neurons. *Cell* **112**, 805-818.

Haag, N., Schwintzer, L., Ahuja, R., Koch, N., Grimm, J., Heuer, H., Qualmann, B. and Kessels, M. M. (2012). The actin nucleator Cobl is crucial for Purkinje cell development and works in close conjunction with the F-actin binding protein Abp1. *J. Neurosci.* **32**, 17842-17856.

Hall, D. H. and Treinin, M. (2011). How does morphology relate to function in sensory arbors? *Trends Neurosci.* **34**, 443-451.

Hatan, M., Shinder, V., Israeli, D., Schnorrer, F. and Volk, T. (2011). The Drosophila blood brain barrier is maintained by GPCR-dependent dynamic actin structures. *J. Cell Biol.* **192**, 307-319.

Hattori, Y., Sugimura, K. and Uemura, T. (2007). Selective expression of Knot/Collier, a transcriptional regulator of the EBF/Olf-1 family, endows the Drosophila sensory system with neuronal class-specific elaborated dendritic patterns. *Genes Cells* **12**, 1011-1022.

Honjo, K., Hwang, R. Y. and Tracey, W. D., Jr (2012). Optogenetic manipulation of neural circuits and behavior in Drosophila larvae. *Nat. Protoc.* **7**, 1470-1478.

Hwang, R. Y., Zhong, L., Xu, Y., Johnson, T., Zhang, F., Deisseroth, K. and Tracey, W. D. (2007). Nociceptive neurons protect Drosophila larvae from parasitoid wasps. *Curr. Biol.* **17**, 2105-2116.

Jan, Y. N. and Jan, L. Y. (2010). Branching out: mechanisms of dendritic arborization. *Nat. Rev. Neurosci.* **11**, 316-328.

Jinushi-Nakao, S., Arvind, R., Amikura, R., Kinameri, E., Liu, A. W. and Moore, A. W. (2007). Knot/Collier and cut control different aspects of dendrite cytoskeleton and synergize to define final arbor shape. *Neuron* **56**, 963-978.

Kania, A., Salzberg, A., Bhat, M., D'Evelyn, D., He, Y., Kiss, I. and Bellen, H. J. (1995). P-element mutations affecting embryonic peripheral nervous system development in Drosophila melanogaster. *Genetics* **139**, 1663-1678.

Kerkhoff, E., Simpson, J. C., Leberfinger, C. B., Otto, I. M., Doerks, T., Bork, P., Rapp, U. R., Raabe, T. and Pepperkok, R. (2001). The Spir actin organizers are involved in vesicle transport processes. *Curr. Biol.* **11**, 1963-1968.

Krupp, J. J., Yaich, L. E., Wessells, R. J. and Bodmer, R. (2005). Identification of genetic loci that interact with cut during Drosophila wing-margin development. *Genetics* **170**, 1775-1795.

Lee, T. and Luo, L. (1999). Mosaic analysis with a repressible cell marker for studies of gene function in neuronal morphogenesis. *Neuron* **22**, 451-461.

Lee, S. B., Bagley, J. A., Lee, H. Y., Jan, L. Y. and Jan, Y. N. (2011). Pathogenic polyglutamine proteins cause dendrite defects associated with specific actin cytoskeletal alterations in Drosophila. *Proc. Natl. Acad. Sci. USA* **108**, 16795-16800.

Li, W., Wang, F., Menut, L. and Gao, F. B. (2004). BTB/POZ-zinc finger protein abrupt suppresses dendritic branching in a neuronal subtype-specific and dosage-dependent manner. *Neuron* **43**, 823-834.

Liu, R., Abreu-Blanco, M. T., Barry, K. C., Linardopoulou, E. V., Osborn, G. E. and Parkhurst, S. M. (2009). Wash functions downstream of Rho and links linear and branched actin nucleation factors. *Development* **136**, 2849-2860.

Longair, M. H., Baker, D. A. and Armstrong, J. D. (2011). Simple Neurite Tracer: open source software for reconstruction, visualization and analysis of neuronal processes. *Bioinformatics* **27**, 2453-2454.

Medina, P. M., Swick, L. L., Andersen, R., Blalock, Z. and Brenman, J. E. (2006). A novel forward genetic screen for identifying mutations affecting larval neuronal dendrite development in Drosophila melanogaster. *Genetics* **172**, 2325-2335.

Meijering, E., Dzyubachyk, O. and Smal, I. (2012). Methods for cell and particle tracking. *Methods Enzymol.* **504**, 183-200.

Nagel, J., Delandre, C., Zhang, Y., Förstner, F., Moore, A. W. and Tavosanis, G. (2012). Fascin controls neuronal class-specific dendrite arbor morphology. *Development* **139**, 2999-3009.

Ohsako, T., Horiuchi, T., Matsuo, T., Komaya, S. and Aigaki, T. (2003). Drosophila lola encodes a family of BTB-transcription regulators with highly variable C-terminal domains containing zinc finger motifs. *Gene* **311**, 59-69.

Ou, Y., Chwalla, B., Landgraf, M. and van Meyel, D. J. (2008). Identification of genes influencing dendrite morphogenesis in developing peripheral sensory and central motor neurons. *Neural Dev.* **3**, 16.

Parrish, J. Z., Kim, M. D., Jan, L. Y. and Jan, Y. N. (2006). Genome-wide analyses identify transcription factors required for proper morphogenesis of Drosophila sensory neuron dendrites. *Genes Dev.* **20**, 820-835.

Pleiser, S., Rock, R., Wellmann, J., Gessler, M. and Kerkhoff, E. (2010). Expression patterns of the mouse Spir-2 actin nucleator. *Gene Expr. Patterns* **10**, 345-350.

Pollard, T. D. and Cooper, J. A. (2009). Actin, a central player in cell shape and movement. *Science* **326**, 1208-1212.

Preibisch, S., Saalfeld, S. and Tomancak, P. (2009). Globally optimal stitching of tiled 3D microscopic image acquisitions. *Bioinformatics* **25**, 1463-1465.

Preibisch, S., Saalfeld, S., Schindelin, J. and Tomancak, P. (2010). Software for bead-based registration of selective plane illumination microscopy data. *Nat. Methods* **7**, 418-419.

Quinlan, M. E., Heuser, J. E., Kerkhoff, E. and Mullins, R. D. (2005). Drosophila Spire is an actin nucleation factor. *Nature* **433**, 382-388.

Riedl, J., Crevenna, A. H., Kessenbrock, K., Yu, J. H., Neukirchen, D., Bista, M., Bradke, F., Jenne, D., Holak, T. A., Werb, Z. et al. (2008). Lifeact: a versatile marker to visualize F-actin. *Nat. Methods* **5**, 605-607.

Ristanović, D., Milosević, N. T. and Stulić, V. (2006). Application of modified Sholl analysis to neuronal dendritic arborization of the cat spinal cord. *J. Neurosci. Methods* **158**, 212-218.

Rosales-Nieves, A. E., Johndrow, J. E., Keller, L. C., Magie, C. R., Pinto-Santini, D. M. and Parkhurst, S. M. (2006). Coordination of microtubule and microfilament dynamics by Drosophila Rho1, Spire and Cappuccino. *Nat. Cell Biol.* **8**, 367-376.

Satoh, D., Sato, D., Tsuyama, T., Saito, M., Ohkura, H., Rolls, M. M., Ishikawa, F. and Uemura, T. (2008). Spatial control of branching within dendritic arbors by dynein-dependent transport of Rab5-endosomes. *Nat. Cell Biol.* **10**, 1164-1171.

Schindelin, J., Arganda-Carreras, I., Frise, E., Kaynig, V., Longair, M., Pietzsch, T., Preibisch, S., Rueden, C., Saalfeld, S., Schmid, B. et al. (2012). Fiji: an open-source platform for biological-image analysis. *Nat. Methods* **9**, 676-682.

Schneider, C. A., Rasband, W. S. and Eliceiri, K. W. (2012). NIH Image to ImageJ: 25 years of image analysis. *Nat. Methods* **9**, 671-675.

Schoenen, J. (1982). Dendritic organization of the human spinal cord: the motoneurons. *J. Comp. Neurol.* **211**, 226-247.

Schumacher, N., Borawski, J. M., Leberfinger, C. B., Gessler, M. and Kerkhoff, E. (2004). Overlapping expression pattern of the actin organizers Spir-1 and formin-2 in the developing mouse nervous system and the adult brain. *Gene Expr. Patterns* **4**, 249-255.

Sholl, D. A. (1953). Dendritic organization in the neurons of the visual and motor cortices of the cat. *J. Anat.* **87**, 387-406.

Smith, C. J., Watson, J. D., Spencer, W. C., O'Brien, T., Cha, B., Albeg, A., Treinin, M. and Miller, D. M., III (2010). Time-lapse imaging and cell-specific expression profiling reveal dynamic branching and molecular determinants of a multi-dendritic nociceptor in C. elegans. *Dev. Biol.* **345**, 18-33.

Spletter, M. L., Liu, J., Liu, J., Su, H., Giniger, E., Komiyama, T., Quake, S. and Luo, L. (2007). Lola regulates Drosophila olfactory projection neuron identity and targeting specificity. *Neural Dev.* **2**, 14.

Stewart, A., Tsubouchi, A., Rolls, M. M., Tracey, W. D. and Sherwood, N. T. (2012). Katanin p60-like1 promotes microtubule growth and terminal dendrite stability in the larval class IV sensory neurons of Drosophila. *J. Neurosci.* **32**, 11631-11642.

Strahler, A. N. (1957). Quantitative analysis of watershed geomorphology. *Transactions – American Geophysical Union* **38**, 913-920.

Sugimura, K., Satoh, D., Estes, P., Crews, S. and Uemura, T. (2004). Development of morphological diversity of dendrites in Drosophila by the BTB-zinc finger protein abrupt. *Neuron* **43**, 809-822.

Thévenaz, P., Ruttimann, U. E. and Unser, M. (1998). A pyramid approach to subpixel registration based on intensity. *IEEE Trans. Image Process.* **7**, 27-41.

Tracey, W. D., Jr, Wilson, R. I., Laurent, G. and Benzer, S. (2003). painless, a Drosophila gene essential for nociception. *Cell* **113**, 261-273.

Tsubouchi, A., Caldwell, J. C. and Tracey, W. D. (2012). Dendritic filopodia, Ripped Pocket, NOMPC, and NMDARs contribute to the sense of touch in Drosophila larvae. *Curr. Biol.* **22**, 2124-2134.

Wellington, A., Emmons, S., James, B., Calley, J., Grover, M., Tolias, P. and Manseau, L. (1999). Spire contains actin binding domains and is related to ascidian posterior end mark-5. *Development* **126**, 5267-5274.

Yan, Z., Zhang, W., He, Y., Gorczyca, D., Xiang, Y., Cheng, L. E., Meltzer, S., Jan, L. Y. and Jan, Y. N. (2013). Drosophila NOMPC is a mechanotransduction channel subunit for gentle-touch sensation. *Nature* **493**, 221-225.

Ye, B., Kim, J. H., Yang, L., McLachlan, I., Younger, S., Jan, L. Y. and Jan, Y. N. (2011). Differential regulation of dendritic and axonal development by the novel Krüppel-like factor Dar1. *J. Neurosci.* **31**, 3309-3319.

Zheng, L. and Carthew, R. W. (2008). Lola regulates cell fate by antagonizing Notch induction in the Drosophila eye. *Mech. Dev.* **125**, 18-29.

Zheng, Y., Wildonger, J., Ye, B., Zhang, Y., Kita, A., Younger, S. H., Zimmerman, S., Jan, L. Y. and Jan, Y. N. (2008). Dynein is required for polarized dendritic transport and uniform microtubule orientation in axons. *Nat. Cell Biol.* **10**, 1172-1180.

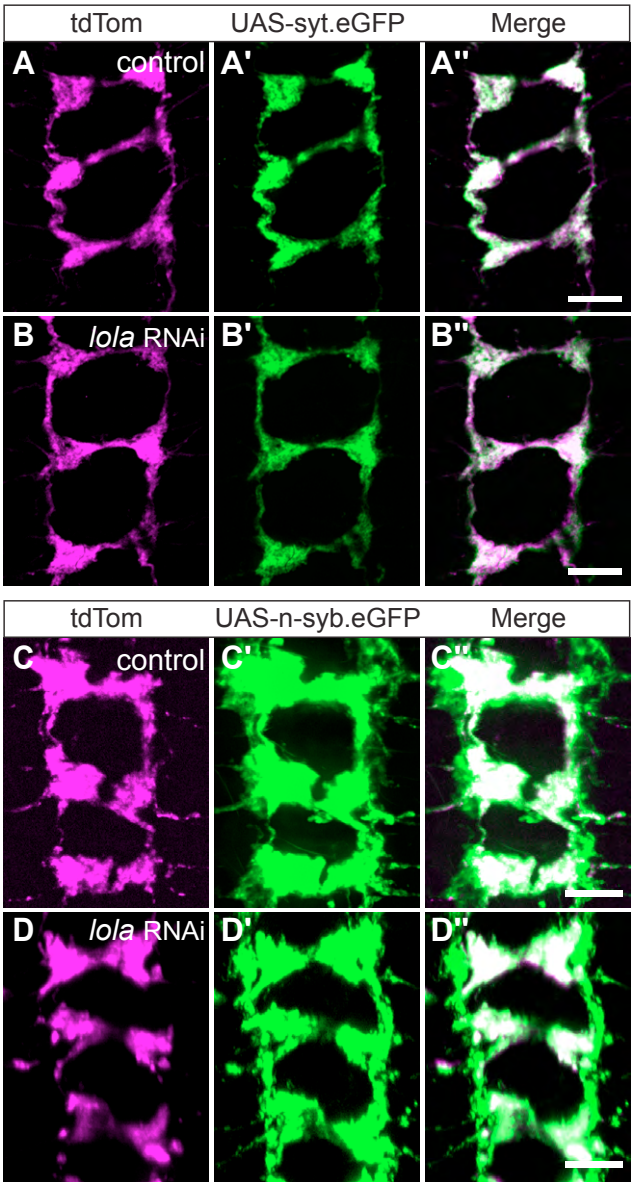

Figure S1. Axon terminals of class IV da neurons appear unaffected by *lola* RNAi in third insta larvae. To label axon terminals of class IV da neurons using *ppk1.9-GAL4,* we used the membrane reporter CD4::tdTomato (tdTom, magenta) or one of two reporters for presynaptic proteins: neuronal synaptotagmin (UAS-syt.eGFP, A',B'), or synaptobrevin (UAS-n-syb.eGFP, C',D'). These markers revealed no overt defects in *lola* RNAi animals. Scale bars: 25µm.

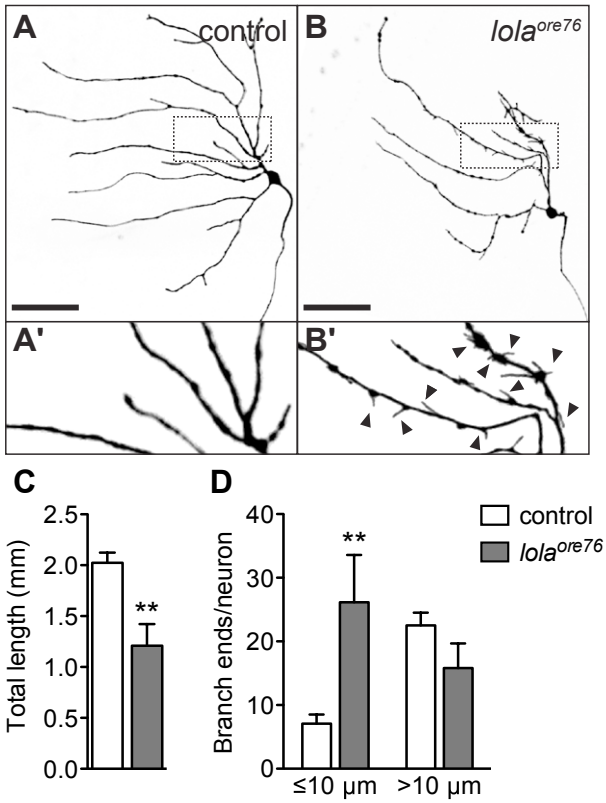

Figure S2. Lola cell autonomously regulates dendrite growth and branching in class I ddaD neurons. (A,B) MARCM clones of Class I ddaD neurons in controls (A) and *lola*^{ore76} (B). Dashed boxes are enlarged in corresponding panels (A',B') to depict the numerous short branches in *lola* mutants (arrowheads). (C,D) Quantifications comparing control (N=10) and *lola*^{ore76} (N=6) clones. (C) Total arbor length (t-test, P=0.0015). (D) Branch number per neuron below (t-test, P=0.0060) or above (t-test, P= 0.1120) a 10µm threshold. Scale bars: 50µm.

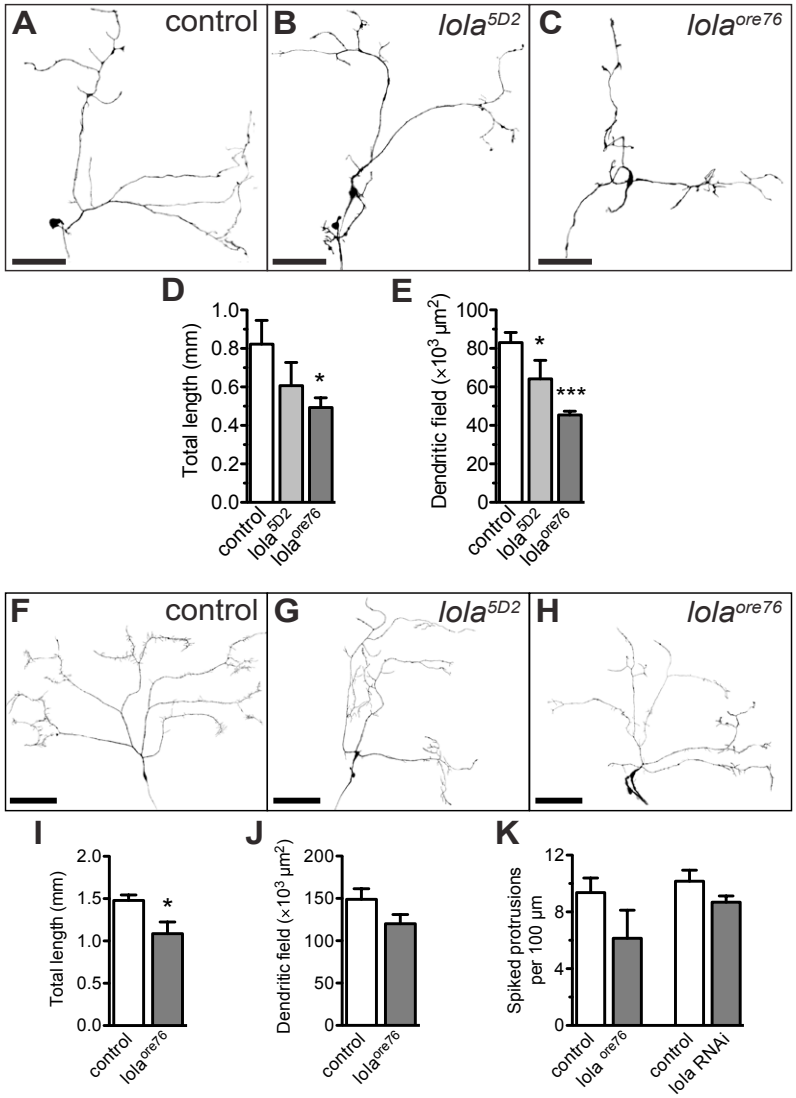

Figure S3. Lola is required for dendrite growth in class II and III da neurons. (A-C) MARCM clones of class II ddaB neurons. (A) Control, (B) *lola*^{5D2} and (C) *lola*^{ore76} ddaB clones showing reduced lengths of major branches. (D,E) Quantifications comparing ddaB controls (N= 7), *lola*^{5D2} clones (N= 3), and *lola*^{ore76} clones (N= 9). (D) Total arbor length (ANOVA, $F_{2,16}$= 3.745, P= 0.0463). (E) Dendritic field (ANOVA, $F_{2,16}$= 22.48, P< 0.0001). (F-K) MARCM clones of class III ddaF neurons. (F) Control, (G) *lola*^{5D2} and (H) *lola*^{ore76} ddaF clones showing decreased arbor length. (I-K) Quantifications comparing ddaF controls (N= 10) and *lola*^{ore76} MARCM clones (N= 4). (I) Total arbor length (t-test, P= 0.0419). (J) Dendritic field (t-test, P= 0.1307). (K) In class III neurons, the density of the spiked protrusions that characterize these arbors was not significantly affected in ddaF MARCM clones (t- test, P= 0.136), nor in ddaA knockdown cells (UAS-*lola*RNAi driven by *tutl*^{GAL4}, a class III specific driver; controls: N= 15, *lola* RNAi: N= 15; t test, P= 0.1056). Scale bars: 100 µm.

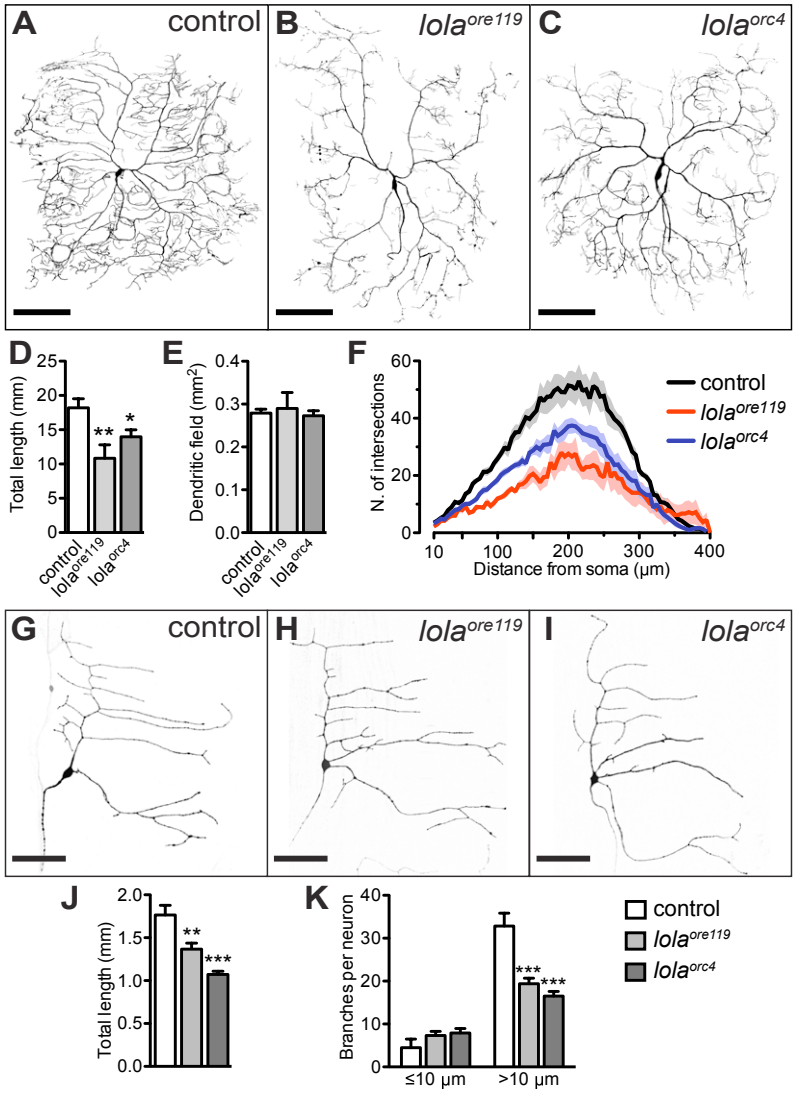

Figure S4. Specific mutations of Lola isoforms L or K reduce dendritic arbors of class IV and class I neurons. (A-F) MARCM clones of the class IV neuron ddaC. (A) Control, (B) *lola*^{ore119} (a mutation in isoform L) and (C) *lola*^{orc4} (a mutation in isoform K) clones. (D-F) Quantifications comparing ddaC controls (N= 12), *lola*^{ore119} clones (N= 5), and *lola*^{orc4} clones (N= 9). (D) Total arbor length (ANOVA, $F_{2,23}$= 9.032, P= 0.0013). (E) Dendritic field (ANOVA, $F_{2,23}$= 0.2666, P= 0.7683). (F) Sholl profiles. (G-I) MARCM clones of the class I neuron ddaE. (J,K) Quantifications comparing ddaE controls (N= 8), *lola*^{ore119} clones (N= 13), and *lola*^{orc4} clones (N= 10). (J) Total arbor length (ANOVA, $F_{2,28}$= 22.18, P< 0.0001). (K) Branch number per neuron below (ANOVA, $F_{2,28}$= 1.365, P= 0.276) or above ($F_{2,28}$= 23.04, P<0.0001) a 10µm threshold. Scale bars: A-C: 100µm; G-I: 50µm.

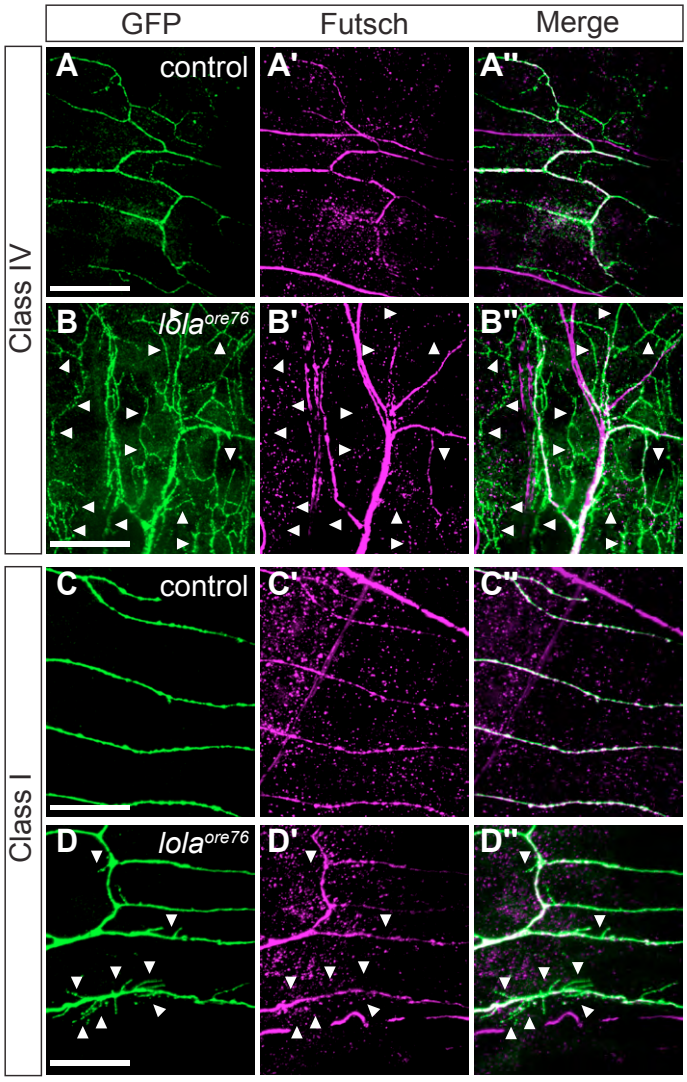

Figure S5. Stable microtubules were virtually absent in ectopic branches of *lola* mutant neurons. (A,B) MARCM clones of class IV ddaC neuron showing distal branches of a control neuron (A) and the proximal bushy arbor of a *lola*^{ore76} clone (B). (A',B') Futsch immunoreactivity was detected in the distal branches of control neuron (A') as well as the proximal thicker arbors of *lola*^{ore76} clone (B'), but was absent from the numerous thinner branches in *lola*^{ore76} (B', arrowheads). (A'',B'') Overlay of GFP and Futsch channels. (C,D) MARCM clones of class I ddaE neuron showing details of the dendritic branches. (C',D') Futsch immunoreactivity was detected in the main branches of both control (C') and *lola*^{ore76} (D') ddaE neuron, but was undetectable in the short branches of *lola*^{ore76} neuron (D', arrowheads). (C'', D'') Overlay of GFP (green) and Futsch (magenta) channels. Scale bars: 25µm.

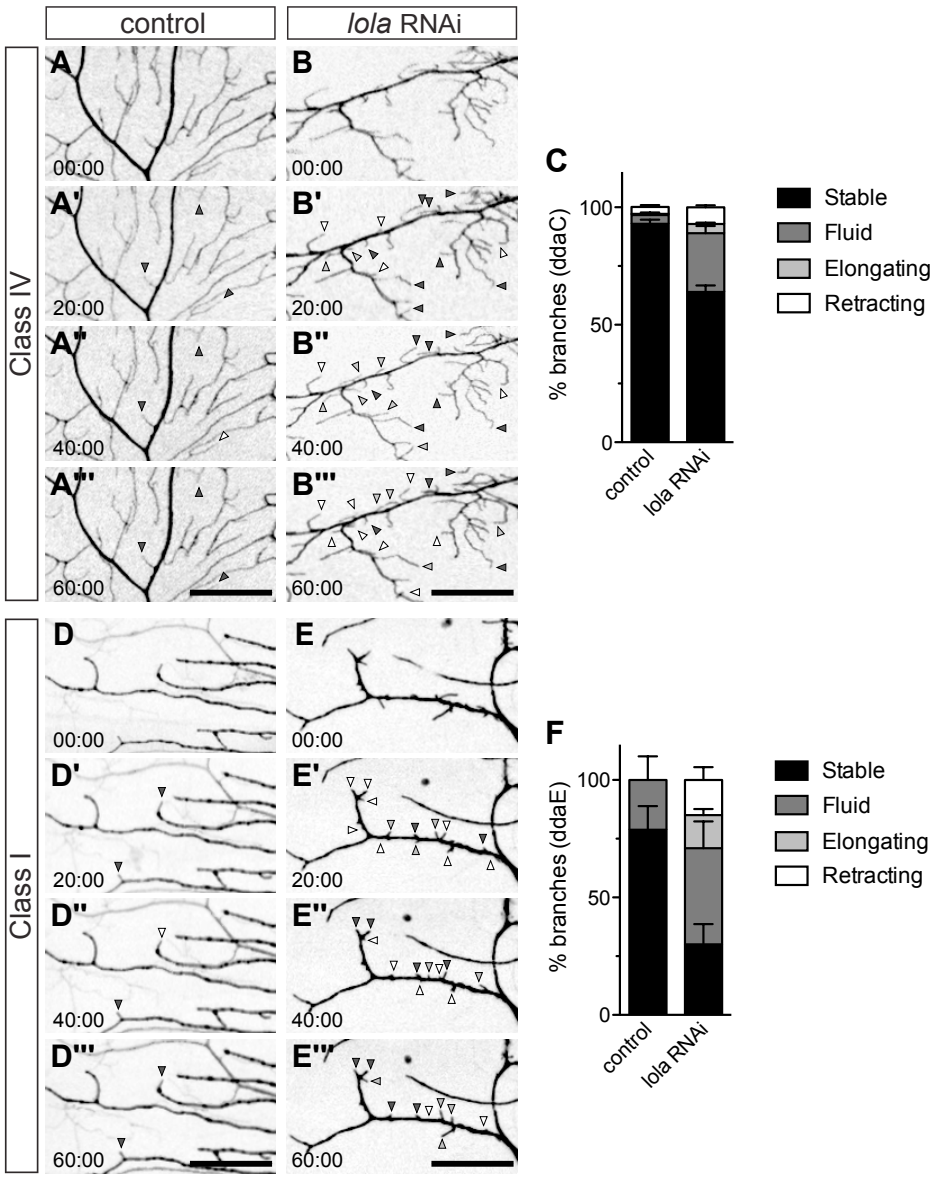

Figure S6. Lola suppresses branch stabilization in late third instar larvae. Branching dynamics revealed by time-lapse confocal images of proximal arbors of late third-instar larvae at 5 min intervals (for simplicity, only every 4th frame is shown). (A-C) Class IV ddaC neurons. (A-A''') The majority of branch ends in the proximal region of control larva (*UAS-Dcr2;;ppk1.9-GAL4,ppk-CD4::tdTomato*) are stable over the period of one hour. (B-B''') In contrast, dendrites in *lola* RNAi larvae (*UAS-Dcr2;UAS-RNAi;ppk1.9-GAL4,ppk-CD4::tdTomato*) exhibit multiple dynamic branching events, including retractions (white arrowheads), extensions (light gray arrowheads), and fluid branches that both extend and retract (dark gray arrowheads). (C) Relative percentages of stable and dynamic branching events, with nearly 1.5 fold reduction in the frequency of stable branches in *lola* RNAi (63.92±3.95) when compared to controls 90.55±2.37). (D-F) Class I ddaE neurons. The numerous short branches in *lola* RNAi are highly dynamic, with nearly threefold reduction in the frequency of stable branches (30.03±12.17) when compared to controls (78.78±14.30). N=2 larvae for each genotype. Scale bars: 25µm. The depicted time-lapses are available as supplemental movies 1 and 2.

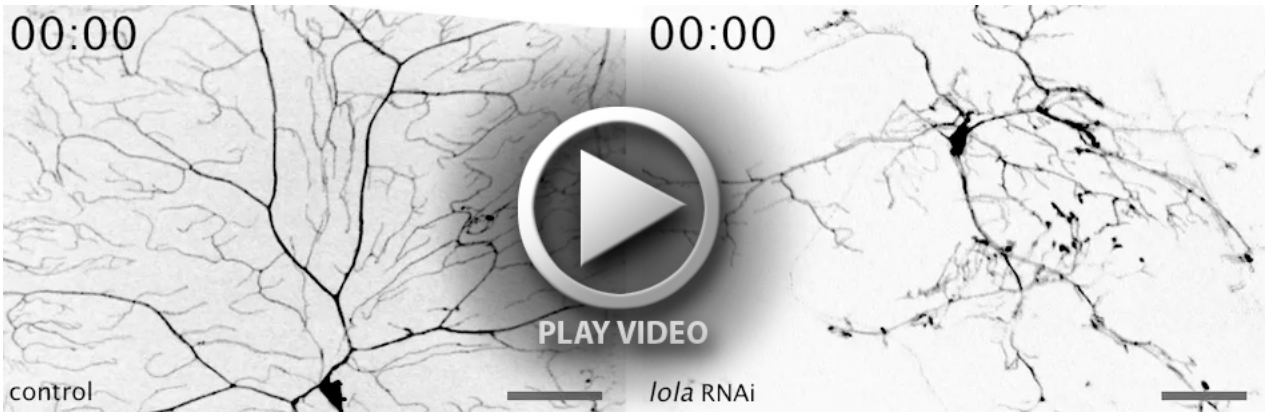

Movie 1. Time-lapse movie of proximal branch dynamics of ddaC class IV neurons at the third instar larval stage. While proximal branches of a representative control larva (left panel, *UAS-Dcr2;;ppk1.9-GAL4,ppk-CD4::tdTomato*) remain stable over the imaging period, *lola* RNAi larva (right panel, *UAS-Dcr2;UAS-RNAi;ppk1.9-GAL4,ppk-CD4::tdTomato*) exhibit multiple dynamic events. The second part of the video repeats the time series while annotating the video-tracked branch ends in the image field. Stacks were acquired every 5 minutes and a maximal projection at each time point used to generate the sequence. Time-stamps are indicated on the upper-left of each panel. While the time series lasts more than one hour, quantifications were restricted to the first hour. Scale bars: 25µm.

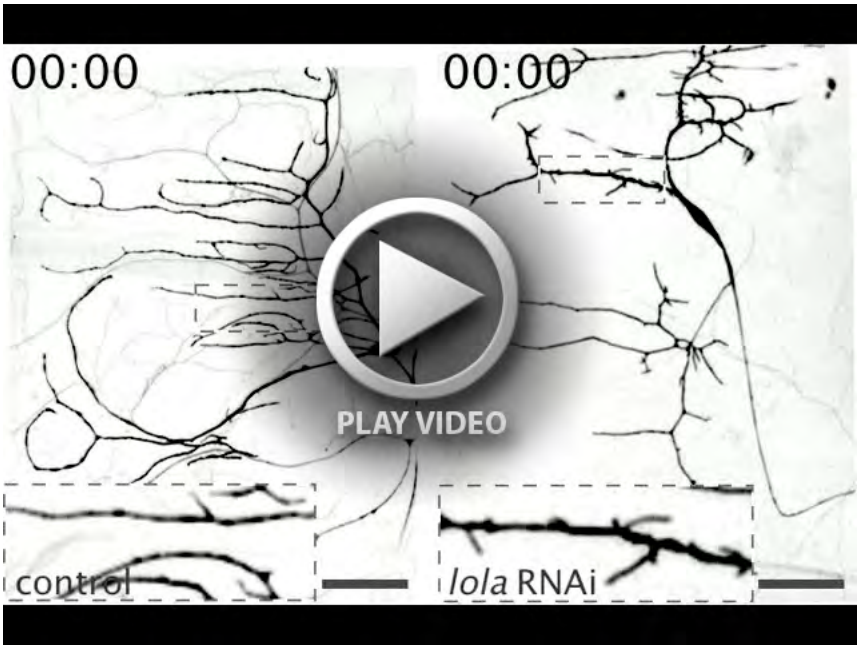

Movie 2. Time-lapse movie of proximal branch dynamics of class I neurons at the third instar larval stage. Most branch ends remain stable in controls (left panel, *UAS-Dcr2;;GAL4^{221},UAS-mCD8::GFP*), but highly dynamic in *lola* RNAi (right panel, *UAS-Dcr2;UAS-RNAi;GAL4^{221},UAS-mCD8::GFP*) animals. Stacks were acquired every 5 minutes and a maximal projection at each time point used to generate the sequence. Time-stamps are indicated on the upper-left of each panel. Dashed boxes are enlarged in corresponding insets. While the time series lasts more than one hour, quantifications were restricted to the first hour. Scale bars: 25µm.